

An alternative approach to train neural networks using monotone variational inequality

Chen Xu^{*1}, Xiuyuan Cheng^{†2}, and Yao Xie^{‡1}

¹H. Milton Stewart School of Industrial and Systems Engineering, Georgia Institute of Technology.

²Department of Mathematics, Duke University

March 13, 2024

Abstract

We propose an alternative approach to neural network training using the monotone vector field, an idea inspired by the seminal work of Juditsky and Nemirovski [Juditsky and Nemirovsky, 2019] developed originally to solve parameter estimation problems for generalized linear models (GLM) by reducing the original non-convex problem to a convex problem of solving a monotone variational inequality (VI). Our approach leads to computationally efficient procedures that converge fast and offer guarantee in some special cases, such as training a single-layer neural network or fine-tuning the last layer of the pre-trained model. Our approach can be used for more efficient fine-tuning of a pre-trained model while freezing the bottom layers, an essential step for deploying many machine learning models such as large language models (LLM). We demonstrate its applicability in training fully-connected (FC) neural networks, graph neural networks (GNN), and convolutional neural networks (CNN) and show the competitive or better performance of our approach compared to stochastic gradient descent methods on both synthetic and real network data prediction tasks regarding various performance metrics.

1 Introduction

Neural Network (NN) training [Duchi et al., 2010, Sutskever et al., 2013, Kingma, 2014, Ioffe and Szegedy, 2015] is the essential process in the study of deep models. Optimization guarantee for training loss, as well as generalization error, have been obtained with over-parameterized networks [Neyshabur et al., 2014, Mei et al., 2018, Arora et al., 2019b,a, Allen-Zhu et al., 2019, Du et al., 2019]. However, due to the inherent non-convexity of loss objectives, theoretical developments are still diffused and lag behind the vast empirical successes.

*cxu310@gatech.edu

†xiuyuan.cheng@duke.edu

‡yao.xie@isye.gatech.edu

Recently, the seminal work [Juditsky and Nemirovsky, 2019] presented a somehow surprising result that some non-convex issues can be circumvented in special cases by problem reformulation. In particular, it was shown that when estimating the parameters of the GLM, instead of minimizing a least-square loss function, which leads to a non-convex optimization problem, no guarantees can be obtained for global convergence nor model recovery, one can reformulate the problem as solving a monotone VI, a general form of convex optimization. The reformulation through monotone VI leads to performance guarantees and computationally efficient procedures.

In this paper, inspired by [Juditsky and Nemirovsky, 2019] and the fact that certain GLM (such as logistic regression) can be viewed as a layer in neural networks, we consider a new scheme for neural network training based on monotone VI. Our approach is a drastic departure from the widely used gradient descent algorithm for neural network training — we replace the gradient of a loss function with a constructed monotone operator to achieve faster convergence, which we demonstrate empirically, and further guaranteed convergence in some special cases, such as one layer neural network or fine-tuning the last layer of a neural network.

Our approach can lead to a more efficient fine-tuning of a pre-trained neural network model: training the last layer and “freezing” the rest of the layers, with fast convergence and guarantee. Fine-tuning has been shown to be effective in leveraging pre-trained models on large datasets for a similar or related task [Liu et al., 2022]. Fine-tuning is a common and essential practice in large language models [Ding et al., 2023] to improve performance over the unmodified pre-trained model on downstream tasks. For some architectures, such as CNN, it is common to keep the earlier layers (those closest to the input layer) frozen because they capture lower-level features. In contrast, upper layers often focus on high-level features that can be more related to the downstream task. In our paper, we demonstrate (i) for fine-tuning the last layer, we can establish training and prediction guarantees – see Section 4; (ii) for fine-tuning the top few (more than one) layers, through extensive numerical studies on synthetic and real-data in Section 6, we demonstrate the faster convergence to a local solution by our approach relative to gradient descent in a comparable setup.

To our knowledge, the current paper is the first to study monotone VI for training neural networks. The proposed SVI, as a general way of modifying the parameter update scheme in NN training, can be applied to various deep architectures. In this work, beyond FC neural networks, we especially study monotone VI training for node classification in GNN [Wu et al., 2019, Pilanci and Ergen, 2020], due to the ubiquity of network data and the importance of network prediction problems. We also study monotone VI training for image classification.

In summary, our technical contributions include:

- Develop a general and practical algorithm for training neural networks using vector field constructed by monotone VI, called *stochastic variational inequality* (SVI). Our work demonstrates the potential power of training neural networks by monotone VI, the idea initially introduced in Juditsky and Nemirovsky [2019] to estimating statistical GLM. The algorithm provides a fundamentally different but easy-to-implement first-order alternative from the commonly used stochastic gradient descent (SGD) of the empirical loss function.

- The computation cost per step is similar between SVI and gradient-based methods. However, training by monotone VI can lead to guarantee in the special case of last-layer training and faster empirical convergence, which is particularly valuable for fine-tuning pre-trained neural network models, as demonstrated by our numerical experiments.
- Compare SVI with widely-used SGD methods to demonstrate that SVI is flexible on various tasks and competitive against SGD, especially the improved efficiency in the early stage of training.

Literature. monotone VI has been studied in priors mainly in the optimization problem context [Kinderlehrer and Stampacchia, 2000, Facchinei and Pang, 2003], which can be viewed as the most general problems with convex structure [Juditsky and Nemirovski, 2022]. More recently, VI has been used to solve min-max problems in Generative Adversarial Networks [Liu et al., 2021] and reinforcement learning [Kotsalis et al., 2022]. In particular, our theory and techniques are inspired by [Juditsky and Nemirovsky, 2019], which uses strongly monotone VI for signal recovery in GLM. In contrast to their work, we thoroughly investigate using VI to train multi-layer NN and address cases when VI may not be strongly monotone.

Meanwhile, our techniques bear similarity to works on “matching loss” [Amid et al., 2022] but are fundamentally different as we leverage monotone VI theory and lead to performance guarantees. On the other hand, we emphasize the difference from [Pilanci and Ergen, 2020], which views two-layer NNs as convex regularizers: we focus on model recovery rather than change variables to convexify the loss minimization. In addition, our SVI extends beyond two-layer networks. Furthermore, a recent work [Combettes et al., 2023] proposed a similar VI-inspired approach in training neural networks, with corresponding convergence guarantees of model parameters. In contrast to our SVI, their proposed method cannot train multiple layers simultaneously, and the technique only demonstrated improved empirical performance over gradient-based methods on training the last layer of a deep neural network.

The rest of the work proceeds as follows. Section 2 introduces general NN setup and provides preliminaries of monotone VI. Section 3 provides the SVI algorithm for training one/last-layer neural networks. Section 4 presents various theoretical guarantees including the prediction performance. Section 5 proposes a heuristic algorithm for training multiple layers, which we demonstrate to work well using numerical examples. Section 6 compares SVI and the SGD on various synthetic and real-data examples to illustrate the potential benefits of SVI. Section 7 concludes the paper. Appendix A contains all proofs.

2 Problem setup

Section 2.1 introduces the general neural network model and GNN notations, and Section 2.2 introduces the monotone VI preliminaries.

2.1 General neural networks

Given N training samples $\{(X^{(i)}, Y^{(i)})\}_{i=1}^N$, where the d -dimensional features $X^{(i)} \in \mathbb{R}^d$, and $Y^{(i)}$ are scalars, which can be real-valued or categorical valued, general neural network learning aims to fit a function

in the data. Suppose the neural network has L -layers, then

$$X_{l+1} = \phi_l(g_l(X_l, \theta_l)), \quad l = 1, \dots, L - 1,$$

denote the nonlinear feature transformation from the previous layer, and $X_1 = X \in \mathbb{R}^d$ is the input with d -dimensional features; $\theta = \{\theta_1, \dots, \theta_L\}$ denotes model parameters, each g_l is the linear “pre-activation.” For example, for fully connected layer, $g_l(x, \theta_l) = W_l^T x + b_l$, and $\theta_l = \{W_l, b_l\}$. Different linear pre-activations can be used depending on the data type, including CNN and GNN layers. Each ϕ_l denotes the activation function at layer l , for example, the sigmoid function $\phi_l(z) = 1/(1 + e^{-z})$. The final output of the neural network is

$$Y = \phi_L(g_L(X_L, \theta_L)).$$

The neural network is a function $f = \phi_L \circ g_L \circ \dots \circ \phi_1 \circ g_1$ with parameter θ , as illustrated in Fig. 1, and \circ in (12) denotes function composition.

For real-valued response, the neural network is typically learned by minimizing the mean-square error loss:

$$\mathcal{L}(\theta) := \frac{1}{N} \sum_{i=1}^N (Y^{(i)} - f(X^{(i)}, \theta))^2. \quad (1)$$

Due to the highly non-linear f , the problem is non-convex. Training neural networks is commonly done by gradient descent, SGD, or other first-order methods using the gradient of the loss function $\mathcal{L}(\theta)$ in (1) with respect to θ .

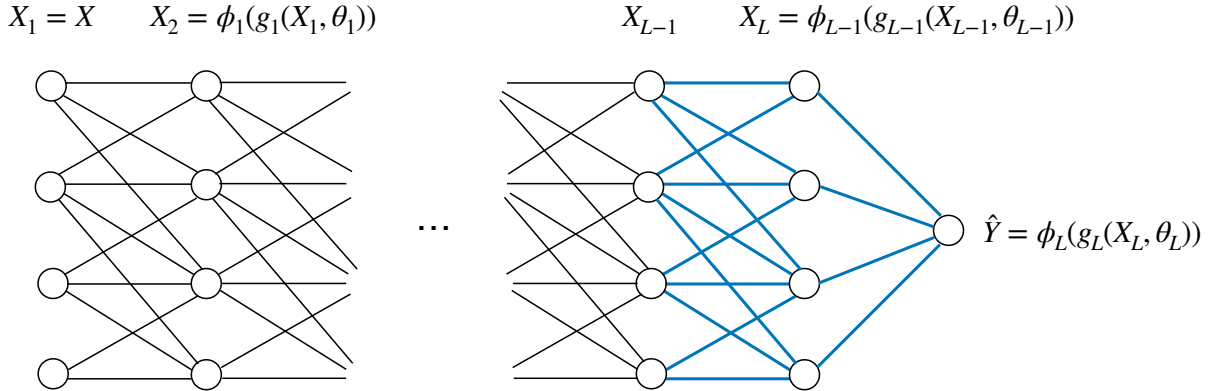


Figure 1: Diagram to show fine-tuning by training the last two layers for a neural network. Black lines indicate frozen parameters and dark green lines indicate parameters to be fine-tuned by training; in this plot, the last two layers are to be trained.

2.2 Preliminaries of monotone VI

We now introduce monotone VI. Given a parameter set $\Theta \subset \mathbb{R}^p$, we call a continuous mapping (operator) $F : \Theta \rightarrow \mathbb{R}^p$ *monotone* if for all $\theta_1, \theta_2 \in \Theta$, $\langle F(\theta_1) - F(\theta_2), \theta_1 - \theta_2 \rangle \geq 0$ [Juditsky and Nemirovsky, 2019].

The operator is called *strongly monotone* with modulus $\kappa > 0$ if for all $\theta_1, \theta_2 \in \Theta$,

$$\langle F(\theta_1) - F(\theta_2), \theta_1 - \theta_2 \rangle \geq \kappa \|\theta_1 - \theta_2\|_2^2. \quad (2)$$

If $F \in C^1(\Theta)$ (i.e., continuously differentiable on Θ) and Θ is closed and convex with non-empty interior, (2) holds if and only if $\lambda_{\min}(\nabla F(\theta)) \geq \kappa$ for all $\theta \in \Theta$, where $\lambda_{\min}(\cdot)$ denotes the minimum eigenvalue of a square matrix.

Now, for a monotone operator F on Θ , the problem called $\text{VI}[F, \Theta]$ is to solve the following

$$\text{Find } \bar{\theta} \in \Theta, \text{ s.t. } \langle F(\bar{\theta}), \theta - \bar{\theta} \rangle \geq 0, \forall \theta \in \Theta. \quad \text{VI}[F, \Theta]$$

It is known that if Θ is compact, then $\text{VI}[F, \Theta]$ has at least one solution [Outrata et al., 2013, Theorem 4.1]. In addition, when Θ is a convex set, then $\text{VI}[F, \Theta]$ is a convex problem, and if $\kappa > 0$ in (2), then $\text{VI}[F, \Theta]$ has exactly one solution [Outrata et al., 2013, Theorem 4.4]. Under mild regularity assumptions, the solution can be solved efficiently to high accuracy, using various iterative schemes such as SGD or the accelerated versions by replacing the gradient with the vector field defined by monotone operator [Juditsky and Nemirovsky, 2019].

3 Monotone VI for last-layer training

We now present the monotone VI-based algorithms for training neural networks. We start with simple one/last-layer network training with monotone VI, where the framework and techniques directly come from [Juditsky and Nemirovsky, 2019], highlighting the similarity/difference with SGD. We then generalize to training multiple-layer neural networks in Section 5.

The motivation for using monotone VI for training is by observing that in each NN layer, the weighted summation and then passing through a monotone non-linear activation can be related to a GLM. Suppose the conditional expectation $\mathbb{E}[Y|X]$ of the response vector is modeled by an L -layer neural network $f(X, \theta)$. We make the following assumption

$$\text{There exists an "ideal model" } \theta^* = \{\theta_1^*, \dots, \theta_L^*\} \text{ such that } \mathbb{E}[Y|X] = f(X, \theta^*).$$

where the expectation is with respect to the conditional distribution of Y on X ; i.e., the best prediction given X on Y that minimizes the mean square error is specified by f with the ideal parameter. Such an assumption can be assumed to be reasonable if f being parameterized by expressive enough neural networks. Note that this can hold for both continuous and categorical responses.

Let us first consider a single-layer neural network (i.e., $L = 1$)

$$g(X, \theta) = \eta(X)\theta, \quad \mathbb{E}[Y|X] = \phi(\eta(X)\theta).$$

for a given feature transformation η from the input X . We construct the monotone operator F as, inspired by

solving GLM in [Juditsky and Nemirovsky, 2019]:

$$F(\theta) := \mathbb{E}_{X,Y} \{ \eta^\top(X) [\phi(\eta(X)\theta) - Y] \}, \quad (3)$$

where z^\top denotes the transpose of z . It can be shown that when ϕ is a monotone function, F is monotone [Juditsky and Nemirovsky, 2019]. We will further explain a few key properties of F in Sec. 4, Lemma 4.1.

Given training samples, we can form a sample version of F using training data, denoted by \widehat{F} . Then, we can train the model using a vector field by monotone operator, which we call the stochastic variational inequality (SVI) algorithm

$$\theta \leftarrow \theta - \gamma \widehat{F}(\theta), \quad (4)$$

where $\gamma > 0$ is the step-size. Due to the monotone vector field property of F , we can prove convergence and guarantee of the training iteration (4) as we show in Section 4. SVI based on (4) differs from SGD, which uses the gradient of a specific loss objective. In SVI, the iteration follows a vector field constructed using the monotone operator \widehat{F} , which does not need to correspond to the gradient of a loss function. Nevertheless, it is known when we minimize a convex objective, \widehat{F} corresponds to the gradient of the objective function: in Section 4.3, we show when minimizing the cross-entropy loss if ϕ is either the sigmoid or softmax, \widehat{F} corresponds to the gradient with respect to parameter θ whereby (4) coincides with SGD.

In the context of fine-tuning the last layer, given an input X to the neural network, $\eta(X) = X_L$, i.e., the feature extracted by previous $L - 1$ “frozen” layers and

$$X_L = \phi_{L-1} \circ g_{L-1} \circ \cdots \circ \phi_1 \circ g_1(X, \theta). \quad (5)$$

This way, we can cast the one/last-layer training as solving a monotone VI, and provide a prediction bound for $\mathbb{E}_X \{ \|f(X, \widehat{\theta}) - f(X, \theta^*)\|_2^2 \}$ for estimator $\widehat{\theta}$ obtained using SVI. When we train the last few layers, we can generalize this approach and present an algorithm in Section 5.

4 Guarantee of monotone VI for last-layer training

We now present guarantees on convergence and recovery of “ideal” parameters for the *last-layer training*. In particular, we consider learning of θ_L when $g_L(X_L, \theta_L) = \eta(X)\theta_L$, where $\eta(X)$ is defined in (5) for last-layer training. In Section 4.1, we can provide an error bound on predicting $\mathbb{E}[Y|X]$ averaged over independent test samples X .

Define the set $\mathcal{D}^{\text{Tr}} := \{(X^{(i)}, Y^{(i)})\}_{i=1}^N$ containing N training samples, and assume the training samples are generated using the “ideal model” with $\theta = \theta^*$. Let $X_{i,L}^*$ be the extracted feature, under the ideal model, from previous $L - 1$ “frozen” layers, following the definition in (5) with the input $X = X^{(i)}$:

$$\eta^*(X^{(i)}) := X_{i,L}^* := \phi_{L-1} \circ g_{L-1} \circ \cdots \circ \phi_1 \circ g_1(X^{(i)}, \theta^*).$$

For the monotone operator $F(\theta_L)$ in (3), consider its empirical version

$$\widehat{F}(\theta_L) = \frac{1}{N} \sum_{i=1}^N X_{i,L}^{*\top} [\phi_L(X_{i,L}^* \theta_L) - Y_i].$$

Let $\widehat{\theta}_L^{(T)}$ denote the learned parameter after T training steps following the SVI iteration (4) using \widehat{F} above. For a new test sample X with featured mapped under the ideal model with first $L - 1$ layers

$$X_L^* = \eta^*(X),$$

we consider the prediction for the test sample X under the learned parameters

$$\widehat{Y}(X, \widehat{\theta}_L^{(T)}) := \phi_L(X_L^* \widehat{\theta}_L^{(T)}). \quad (6)$$

The prediction (6) will be measured against the ideal model prediction $\mathbb{E}[Y|X] = f(X, \theta^*)$.

We first state a few properties of $F(\theta_L)$ defined in (3) using $\eta^*(X)$, i.e., the feature mapped using ideal model and identify the form of κ .

Lemma 4.1. *Assume $\phi_L : \mathbb{R}^p \rightarrow \mathbb{R}^p$ is K -Lipschitz continuous and monotone on its domain. For arbitrary test sample X , $F(\theta_L)$ is monotone with modulus κ and K_2 -Lipschitz, where $K_2 = K \mathbb{E}_X \{\|\eta^*(X)\|_2^2\}$, and*

$$\kappa = \lambda_{\min}(\nabla \phi_L) \lambda_{\min}(\mathbb{E}_X [\eta^*(X)^\top \eta^*(X)]). \quad (7)$$

Moreover, $F(\theta_L^*) = 0$.

The property $F(\theta_L^*) = 0$ implies that the ideal last-layer model parameter θ_L^* is a solution to $\text{VI}[F, \Theta]$ constructed for the last-layer. In particular, if $\kappa > 0$, it is the *unique* solution. As a result, θ_L^* can be efficiently solved to a high accuracy using $F(\theta_L)$ under appropriated chosen γ . the precise statement is provided in Section 4.1.

4.1 Case 1: modulus $\kappa > 0$

Under appropriate step size selection and additional regularity assumptions, we can obtain bounds on the recovered parameters following techniques in [Juditsky and Nemirovsky, 2019], which further enables us to bound the error of model prediction. Note that the guarantee relies on κ , which may be estimated using N training samples.

Lemma 4.2 (Parameter recovery guarantee). *Suppose that there exists $M < \infty$ such that $\forall \theta \in \Theta$,*

$$\mathbb{E}_{X, Y(\theta)} \|X_L^* Y(\theta)\|_2 \leq M,$$

where $\mathbb{E}[Y(\theta)|X] = \phi_L(X_L^* \theta)$. Choose adaptive step sizes $\gamma_t = [\kappa(t + 1)]^{-1}$ in (4). Then the sequence of

estimators $\widehat{\theta}_L^{(T)}$ obeys the error bound

$$\mathbb{E}_{\mathcal{D}^{\text{Tr}}}\{\|\widehat{\theta}_L^{(T)} - \theta_L^*\|_2^2\} \leq \frac{4M^2}{\kappa^2(T+1)}. \quad (8)$$

Above, the expectation is with respect to the randomness of training data, since $\widehat{\theta}_L^{(T)}$ depends on training data \mathcal{D}^{Tr} .

One implication of the lemma is that the convergence rate of the algorithm depends on the smallest eigenvalue of the covariance matrix of the extracted features $\theta(X)$; if the extracted features after $L - 1$ -layers are more uncorrelated with each other, the smallest eigenvalue will be larger. We will show numerically that, in practice, the performance depends on the smallest eigenvalue of the sample covariance matrix of $\theta(X)$ and, thus, depends on the sample size.

We can use the Lemma 4.2 to bound the prediction error as below.

Theorem 4.3 (Prediction error using strongly monotone F). *Given a test sample X , the expected prediction error by (6) is bounded by*

$$\mathbb{E}_{(X, \mathcal{D}^{\text{Tr}})}\{\|\widehat{Y}(X, \widehat{\theta}_L^{(T)}) - \mathbb{E}[Y|X]\|_2^2\} \leq \frac{C_t}{T+1},$$

where $C_t = 4M^2K^2\lambda_{\max}(\mathbb{E}_X[X_L^{*\top}X_L^*]) \cdot \kappa^{-2}$, and the expectation is with respect to the randomness of training samples and test sample, respectively.

Note that $p = 2$ yields the sum-of-squared error bound on prediction, and $p = \infty$ yields an entry-wise bound. Additionally, the proof of Theorem 4.3 only requires access to an unbiased estimator of F , so that the batch size can range from one to N , where N is the size of the training data.

Remark 4.4 (When does $\kappa > 0$?). Recall that the modulus κ is defined as (7). To have $\lambda_{\min}(\mathbb{E}_X[X_L^{*\top}X_L^*])$ is bounded away from zero, we thus are concerned with the minimum eigenvalue of the gradient of ϕ acting on its inputs. Note that the Jacobian matrix is diagonal when ϕ_L is an element-wise function on its vector inputs. In this case, we only need the element-wise activation function to be continuously differentiable with positive derivatives; for instance, the sigmoid function, for any $y \in \mathbb{R}^p$

$$\lambda_{\min}[\nabla\phi_L]|_y = \min_{i=1, \dots, p} \phi_L(y_i)(1 - \phi_L(y_i)),$$

which is bounded away from zero. However, the ReLu function does not satisfy this requirement.

4.2 Case 2: modulus $\kappa = 0$

In practice, we may encounter cases where the operator F is only monotone but not strongly monotone. For instance, when ϕ is the softmax function that applied element-wise to $\eta^*(X)\theta_L \in \mathbb{R}^{n \times F}$, the Jacobian matrix is block-diagonal. For any vector $z \in \mathbb{R}^F$, $\nabla\phi(z) = \text{diag}(\phi(z)) - \phi(z)\phi(z)^T$, which satisfies

$\nabla\phi(z)\mathbf{1} = \mathbf{0}$ for any z [Gao and Pavel, 2018, Proposition 2]. Therefore, the minimum eigenvalue of the gradient matrix of ϕ is always zero, and hence $\kappa = 0$.

In this case, note that the solution of $\text{VI}[F, \Theta]$ needs not be unique: a solution $\bar{\theta}_L$ that satisfies the condition $\langle F(\bar{\theta}_L), \theta - \bar{\theta}_L \rangle \geq 0, \forall \theta \in \Theta$ may not correspond to the ideal θ_L^* (so there is no identifiability). Nevertheless, we directly approximate the zero of F by using the operator extrapolation method (OE) in [Kotsalis et al., 2022]. We then have an ℓ_p bound on prediction error:

Theorem 4.5 (Prediction error using monotone F). *Suppose we run the OE algorithm [Kotsalis et al., 2022] for T iterations with $\lambda_t = 1, \gamma_t = 1/(4K_2)$, where K_2 is the Lipschitz constant of F . Let R be uniformly chosen from $\{2, 3, \dots, T\}$. Then*

$$\mathbb{E}_{\mathcal{D}^{\text{Tr}}}\{\|\mathbb{E}_X\{\sigma_{\min}(\eta^*(X)^\top)[\widehat{Y}(X, \widehat{\theta}_L^{(R)}) - \mathbb{E}[Y|X]]\}\|_2\} \leq \frac{C_t''}{\sqrt{T}},$$

where $\sigma_{\min}(\cdot)$ denotes the minimum singular value of its input matrix and the constant $C_t'' = 3\sigma + 12K_2(2\|\theta_L^*\|_2^2 + 2\sigma^2/L^2)^{1/2}$, in which $\sigma^2 = \mathbb{E}_{\mathcal{D}^{\text{Tr}}}[(\widehat{F}(\theta_L) - F(\theta_L))^2]$ is the variance of the unbiased estimator $\widehat{F}(\theta_L)$.

The convergence rate in Theorem 4.5 is unaffected by the batch size, which only serves to reduce the variance. In addition, Theorem 4.5 requires R be uniformly chosen from $\{2, 3, \dots, T\}$, so that the theoretical guarantee holds at a random training epoch. In theory, this assumption is necessary to ensure a decrease of the norm of the monotone operator ([Kotsalis et al., 2022], Eq. (3.20)). In practice, we observed that the epoch that leads to the highest validation accuracy might not occur at the end of T training epochs, so this assumption is reasonable based on empirical evidence.

4.3 Special cases: Monotone operator vector field becomes gradient

In practice, neural networks are commonly trained via empirical loss minimization, in contrast to solving the monotone VI approach here. Nevertheless, it can be shown that if not solving minimizing the mean-square-error as in (1), but instead using the cross-entropy loss when ϕ is either the sigmoid function or the softmax function, the monotone operator F defined in (3) will correspond to the expectation of the gradient of the loss with respect to parameters. As a result, the two approaches (SGD and SVI) yield the same last-layer training algorithm.

Consider a pair of input $X \in \mathbb{R}^d$ and output $Y \in \{0, \dots, k\}$. Let $e_Y \in \{0, 1\}^{k+1}$ be the one-hot encoding of Y . Now, the cross-entropy loss $\mathcal{L}(\theta_L)$ is

$$\mathcal{L}(\theta_L) = -Y \log(\phi_L(\eta^*(X)\theta_L)) - (1 - Y) \log(1 - \phi_L(\eta^*(X)\theta_L)), \quad Y \in \{0, 1\}. \quad (9)$$

$$\mathcal{L}(\theta_L) = -e_Y^T \log(\phi_L(\eta^*(X)\theta_L)), \quad Y \in \{0, \dots, k\}, k > 1. \quad (10)$$

In binary classification (9), $\phi_L(x) = 1/(1 + e^{-x})$ is the element-wise sigmoid function. In multi-class classification (10) $\phi_L(x) = [e^{x_1}/\sum_j e^{x_j}, \dots, e^{x_{k+1}}/\sum_j e^{x_j}]$ is the softmax function. We now have the

following proposition.

Proposition 4.6 (The equivalence between SVI and parameter gradient). *Under the setup for (9) or (10), we have that for any $\theta_L \in \Theta$*

$$\mathbb{E}_{X,Y}[\nabla_{\theta_L} \mathcal{L}(\theta_L)] = F(\theta_L),$$

where the monotone operator $F(\theta_L)$ is defined in (3), and the expectation is with respect to randomness in both input X and output Y .

5 Extension: Training multiple last layers

Now we look into generalizing the last one-layer training by considering training the last few layers of a network, from layer L' to L , $1 \leq L' \leq L$, and typically the number of trained layers $L - L' \geq 1$ is small. We will show how to construct the vector field based on (3). Specifically, we aim to design $F_l(\theta_l)$, $l = L', \dots, L$, for parameters θ_l in layer l of the neural network, similar to the scheme before, and use these $F_l(\theta_l)$ as update directions for the parameters $\{\theta_l\}_{l=L'}^L$ in training by (4).

However, there are several difficulties in directly extending $F(\theta)$ in (3) to train multi-layer neural networks. First; the definition assumes that the pre-activation mapping $\eta(X)\theta$ is linear with respect to θ . This linearity assumption does not hold for many types of network layers. Second, more importantly, the monotone operator (3) is defined using Y , the observation of the response variable. However, such observation is unavailable when we define $F_l(\theta_l)$ for intermediate layers, where Y_l would denote the ‘‘true’’ value to be approximated by outputs from the l -th hidden layer. Third, how to generalize (3) for different loss objectives is unclear. Thus, we will build a heuristic proven to be good in practice.

5.1 Revisit single-layer training

To motivate the monotone VI-inspired scheme designed for multiple last-layer training, we first present a mathematically equivalent view of $F(\theta)$ in (3) for single-layer training. Consider for the last layer of the

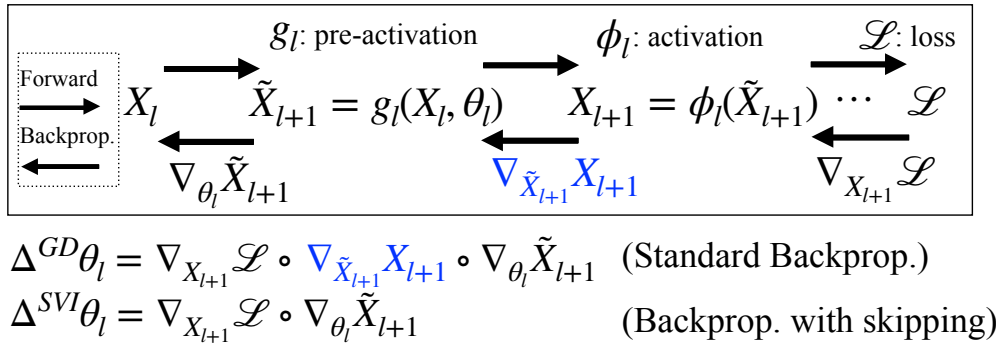


Figure 2: Gradient descent (GD) vs. SVI for fine-tuning an arbitrary layer l , $L' \leq l \leq L$, via *backward unrolling scheme*: the difference lies in the skipping of differentiation of the activation ϕ with respect to pre-activation values. The notation \circ denotes function composition.

neural network, the linear pre-activation mapping for input $\eta(X)$ (feature mapped from the previous layers), with parameter θ

$$\tilde{X}(\theta) = \eta(X)\theta.$$

Note that the $\tilde{X}(\theta)$ does not need to depend on θ linearly, although in most neural networks the dependence is linear. The corresponding prediction is given by $\hat{Y} = \phi(\tilde{X})$, and consider the mean-squared-error (MSE) loss:

$$\mathcal{L}(\hat{Y}, Y) = \frac{1}{2} \|\hat{Y} - Y\|_2^2. \quad (11)$$

Recall, by our construction, the vector field can also be written as

$$\begin{aligned} F(\theta) &:= \mathbb{E}_{X,Y} \{ \eta^\top(X) [\hat{Y} - Y] \} \\ &= \mathbb{E}_{X,Y} \{ \nabla_{\hat{Y}} \mathcal{L} \circ \nabla_{\theta} \tilde{X}(\theta) \}, \end{aligned} \quad (12)$$

where the last equality is due to $\nabla_{\hat{Y}} \mathcal{L} = (\hat{Y} - Y)$, $\nabla_{\theta} \tilde{X}(\theta) = \eta^\top(X)$. Thus, this observation says that the monotone operator vector field can be constructed as the product of two terms: where the first term in (12), $\nabla_{\hat{Y}} \mathcal{L}$, the gradient of the loss objective with respect to the network prediction \hat{Y} says the sensitivity of the loss regarding the network prediction \hat{Y} , and the second term $\nabla_{\theta} \tilde{X}$ is the gradient of the *pre-activation* mapping \tilde{X} with respect to the parameter θ , which due to linearity is the input of the network.

5.2 Backward unrolling scheme for multi-layer training

Based on this observation from (12), we propose SVI for multiple layer training based on a *backward unrolling scheme* as in Algorithm 1 and illustrated in Figure 2. For notational simplicity, we present the scheme for a single data point (X, Y) , and the actual algorithm can use the average over multiple samples:

- For a L -layer network, to tune the last layer, since

$$\mathcal{L} = \frac{1}{2} \left\| \underbrace{\phi_L \circ g_L}_{\hat{Y}}(X_L) - Y \right\|_2^2,$$

we can directly use (12) by treating the input of last layer as $\eta(X) = X_L$: the mapping of original input X into features using all first $L - 1$ layers, and \hat{Y} is the prediction by forward predict passing the input $\eta(X)$ through the last layer.

- Now, to train the $L - 1$ layer's weights while fixing the L th layer, we note that the loss can be written as

$$\mathcal{L} = \frac{1}{2} \left\| \phi_L \circ g_L \circ \underbrace{\phi_{L-1} \circ g_{L-1}}_{X_L}(X_{L-1}) - Y \right\|_2^2$$

where we can use $\eta(X) = X_{L-1}$ as the features learned by the previous $L - 2$ layers, and use the sensitivity of the loss with respect to the output of the $(L - 1)$ th layer, X_L , in the construction of the monotone operator vector field, $\nabla_{X_L} \mathcal{L} = \nabla_z \left(\frac{1}{2} \|\phi_L \circ g_L(z)\|_2^2 \right)$.

- In general, to train layers from l , $L' \leq l \leq L$, we notice that

$$\mathcal{L} = \frac{1}{2} \|\phi_L \circ g_L \cdots \circ \phi_l \circ g_l(X_l) - Y\|_2^2,$$

using the idea to construct the monotone VI vector field by using $\eta(X) = X_L$, we can use (12) with $\eta(X) = X_l$, and

$$\nabla_{X_{l+1}} \mathcal{L} = \nabla_z \left(\frac{1}{2} \|\phi_L \circ g_L \cdots \circ \phi_{l+1} \circ g_{l+1}(z)\|_2^2 \right) \quad (13)$$

Note that compared to the commonly used gradient $\nabla_{\theta} \mathcal{L}$ in backpropagation, Algorithm 1 only differs by *skipping* the derivative of the point-wise non-linearity ϕ with respect to its input. Therefore, SVI has a similar computational cost against gradient-based methods. In practice, this skipping leads to different dynamics when updating neurons in the network; see Remark 5.1 for details.

5.3 Practical considerations

The approach taken in Algorithm 1 has two main benefits. First, it addresses the challenges of extending monotone VI to multi-layer training. More precisely, the Algorithm applies to arbitrary forms of network layers $g_l(X_l, \theta_l)$, nonlinear activations ϕ_l , and the loss function \mathcal{L} . It also requires no observation of responses from neurons in hidden layers. Second, it is easy to implement by leveraging automatic differentiation [Paszke et al., 2017]. Specifically, we implement the skipping idea via backpropagating the layer-wise surrogate loss $\tilde{\mathcal{L}}_l$ with respect to θ_l . Note that this loss $\tilde{\mathcal{L}}_l$ is simple to compute: the quantity \tilde{X}_{l+1} is available during the forward pass on training data X , and gradients $\nabla_{X_{l+1}} \mathcal{L}$ are available upon backpropagating the original loss \mathcal{L} with respect to outputs of each layer l .

Remark 5.1 (Effect on training dynamics). We remark on a key difference between parameter update in SGD and in SVI, which ultimately affects training dynamics. Suppose the activation function is ReLU. It is well-known that SGD does not update weights of *inactive neurons* (i.e., $\text{ReLU}(x) = 0$) because the gradient of ReLU with respect to them is zero. However, SVI does not discriminate between active and inactive neurons as it *skips* this derivative computation. Thus, one can expect that SVI results in a more significant weight update than SGD, which experimentally seems to speed up the initial model convergence. We illustrate this phenomenon in Figure 5.

Remark 5.2 (Implementation caveats). We have two remarks that help avoid incorrect implementation when SVI is implemented in existing software (e.g., PyTorch Paszke et al. [2019]). First, before obtaining $\{\nabla_{X_{l+1}} \mathcal{L}\}_{l=1}^L$ in line 5, model parameters $\{\theta_l\}$ should not require gradients. Otherwise, the backpropagation of the original loss to obtain $\{\nabla_{X_{l+1}} \mathcal{L}\}_{l=1}^L$ would also store gradients of \mathcal{L} with respect to θ before the SVI updates. Second, after obtaining $F_l^{(i)}(\theta_l)$ in line 8, θ_l should not require gradient (until the next for loop in line 6 is called). Otherwise, because \tilde{X}_{l+2} as the output by the $(l+1)$ -th layer implicitly depends on θ_l , backpropagating the surrogate loss $\tilde{\mathcal{L}}$ with respect to model parameters would incorrectly accumulate update directions for θ_l .

Algorithm 1 Stochastic variational inequality (SVI) with backward unrolling scheme

Input: (a) Training data $\{(X^{(i)}, Y^{(i)})\}_{i=1}^N$, (b) L -layer network $f(X, \theta) = \{\phi_l \circ g_l(X_l, \theta_l)\}_{l=1}^L$, (c) Loss function \mathcal{L} , (d) Learning rate $\gamma > 0$, (e) desired $L' \in [1, L - 1]$ (f) Number of steps S

Output: Trained model parameters $\hat{\theta} = \{\hat{\theta}_l\}_{l=L'}$

- 1: Initialize the network with $\hat{\theta}$
 - 2: **for** update step $s = 1, \dots, S$ **do**
 - 3: **for** each training sample $i = 1, \dots, N$ **do**
 - 4: Store $\{(\tilde{X}_{l+1}, X_{l+1})\}_{l=L'}^L$ with input $X^{(i)}$: $\tilde{X}_{l+1} = g_l(X_l, \hat{\theta}_l)$ and $X_{l+1} = \phi_l(\tilde{X}_{l+1})$
 - 5: Obtain $\{\nabla_{X_{l+1}} \mathcal{L}\}_{l=L'}^L$ defined in (13)
 - 6: **for** Layer $l = L', \dots, L$ **do**
 - 7: Compute the surrogate loss $\tilde{\mathcal{L}}_l = \langle \nabla_{X_{l+1}} \mathcal{L}, \tilde{X}_{l+1} \rangle$
 - 8: Obtain $F_l^{(i)}(\theta_l) = \nabla_{X_{l+1}} \mathcal{L} \circ \nabla_{\theta_l} \tilde{X}_{l+1} = \nabla_{\theta_l} \tilde{\mathcal{L}}_l$
 - 9: **end for**
 - 10: **end for**
 - 11: Update $\hat{\theta}_l = \hat{\theta}_l - \gamma \left(\frac{1}{N} \sum_{i=1}^N F_l^{(i)}(\theta_l) \Big|_{\theta_l = \hat{\theta}_l} \right)$ for $l = L', \dots, L$
 - 12: **end for**
-

Remark 5.3 (Extension to GNN). Our approach can also be extended for special neural network architectures, such as GNN and CNN. Below we remark on how to extend to GNN. Suppose we have an undirected and connected graph $\mathcal{G} = (\mathcal{V}, \mathcal{E}, W)$, where \mathcal{V} is a finite set of n vertices, \mathcal{E} is a set of edges, and $W \in \mathbb{R}^{n \times n}$ is a weighted adjacency matrix that encodes node connections. Let I_n denote an identity matrix of size n . Let D be the degree matrix of W and $L_g = I_n - D^{-1/2} W D^{-1/2}$ be the normalized graph Laplacian, which has the eigen-decomposition $L_g = U \Lambda U^T$. For a graph signal $X \in \mathbb{R}^{n \times d}$ with d input channels, it is then filtered via pre-activation function in the form of $g_l(L_g, \theta_l)$ which acts on L_g with channel-mixing parameters $\theta_l \in \mathbb{R}^{d \times k}$ for k output channels. Thus, the filtered signal in the l -th layer is given by $X' = g_l(L_g, \theta_l) X$. It is common that $g_l(L_g, \theta_l) X = \eta(X) \theta_l$, where $\eta(X) = \sum_{r=1}^R h_r(L_g) X$ is the sum of R fixed graph filters determined by graph Laplacian L_g [Kipf and Welling, 2017, Defferrard et al., 2016, Hamilton et al., 2017].

6 Experiments

We test and compare SVI in Algorithm 1 with SGD on several synthetic and real-data experiments, where the networks vary in width and depth. We aim to demonstrate the benefits of SVI in terms of reaching faster convergence and competitive/better final performance¹.

6.1 Result summary

Below is a summary of the experiments we performed in this section.

One-layer networks (Sec. 6.3.1): We provided theoretical guarantees in Section 4. When data are generated from a non-convex probit model, SVI outperforms SGD with smaller test losses and higher prediction

¹The code is available at <https://github.com/hamrel-cxu/SVI-NN-training>.

accuracies.

Two-layer networks (Sec. 6.3.2): SVI reaches smaller losses and errors than SGD throughout training epochs. Specifically, we observe performance gains on graphs with varying sizes (i.e., the number of graph nodes ranges from 15 to 600).

Three-layer networks (Sec. 6.4.1 and 6.4.2): On real solar and traffic data, SVI almost always reaches smaller classification error and higher weighted F_1 scores than SGD, in addition to faster initial convergence by SVI.

Networks with more than three layers, using CNN and GNN (Sec. 6.4.3 and 6.4.4): We compare SVI and SGD on node classification for large graphs and image classification. The node classification task uses one large-scale realistic node classification dataset from the Open Graph Benchmark [Hu et al., 2020]. The image classification uses the MNIST [LeCun, 1998] and CIFAR-10 [Krizhevsky et al., 2009] datasets. In particular, the results show that SVI yields improved efficiency during the initial stages of training and reaches competitive overall training performances.

6.2 Setup and comparison metrics

Setup. All implementation are done using `PyTorch` [Paszke et al., 2019] and `PyTorch Geometric` [Fey and Lenssen, 2019] (for GNN). To ensure a fair comparison, we carefully describe the experiment setup. In particular, the following inputs are *identical* to both SVI and SGD in each experiment.

- Data: (a) the size of training and test data (b) batch (batch size and samples in mini-batches).
- Model: (a) architecture (e.g., layer choice, activation function, hidden neurons) (b) loss function.
- Training regime: (a) parameter initialization (b) hyperparameters for backpropagation (e.g., learning rate) (c) total number of epochs.

Thus, all except the update directions for parameters are kept the same for a fair comparison: our SVI uses $F_l(\theta_l)$ in Algorithm 1 and SGD uses the gradient of the loss with respect to parameters.

Comparison metrics. Consider inputs $X \in \mathbb{R}^{n \times d}$, where n is the number of graph nodes (when the data are vectors, we have $n = 1$) and d is the feature dimension per node. Let the true (or predicted) model be $\mathbb{E}[Y|X, \theta] \in \mathbb{R}^{n \times k}$ (or $\mathbb{E}[Y|X, \hat{\theta}]$), where k is the output dimension per node. Given N samples $\{(X^{(i)}, Y^{(i)})\}_{i=1}^N$, we consider the following metrics.

$$\text{MSE loss} = \frac{1}{N} \sum_{i=1}^N \|\mathbb{E}[Y^{(i)}|X^{(i)}, \hat{\theta}] - Y^{(i)}\|_2 \quad (14)$$

$$\text{Cross-entropy loss} = \frac{1}{N} \sum_{i=1}^N \langle Y^{(i)}, -\log(\mathbb{E}[Y^{(i)}|X^{(i)}, \hat{\theta}]) \rangle \quad (15)$$

$$\text{Classification error} = \frac{1}{nNk} \sum_{i=1}^N \sum_{j=1}^n \sum_{f=1}^k \mathbf{1}(Y_{j,f}^{(i)} \neq \hat{Y}_{j,f}^{(i)}) \quad (16)$$

$$\ell_2 \text{ model recovery error} = \frac{1}{N} \sum_{i=1}^N \|\mathbb{E}[Y^{(i)}|X^{(i)}, \hat{\theta}] - \mathbb{E}[Y^{(i)}|X^{(i)}, \theta]\|_2. \quad (17)$$

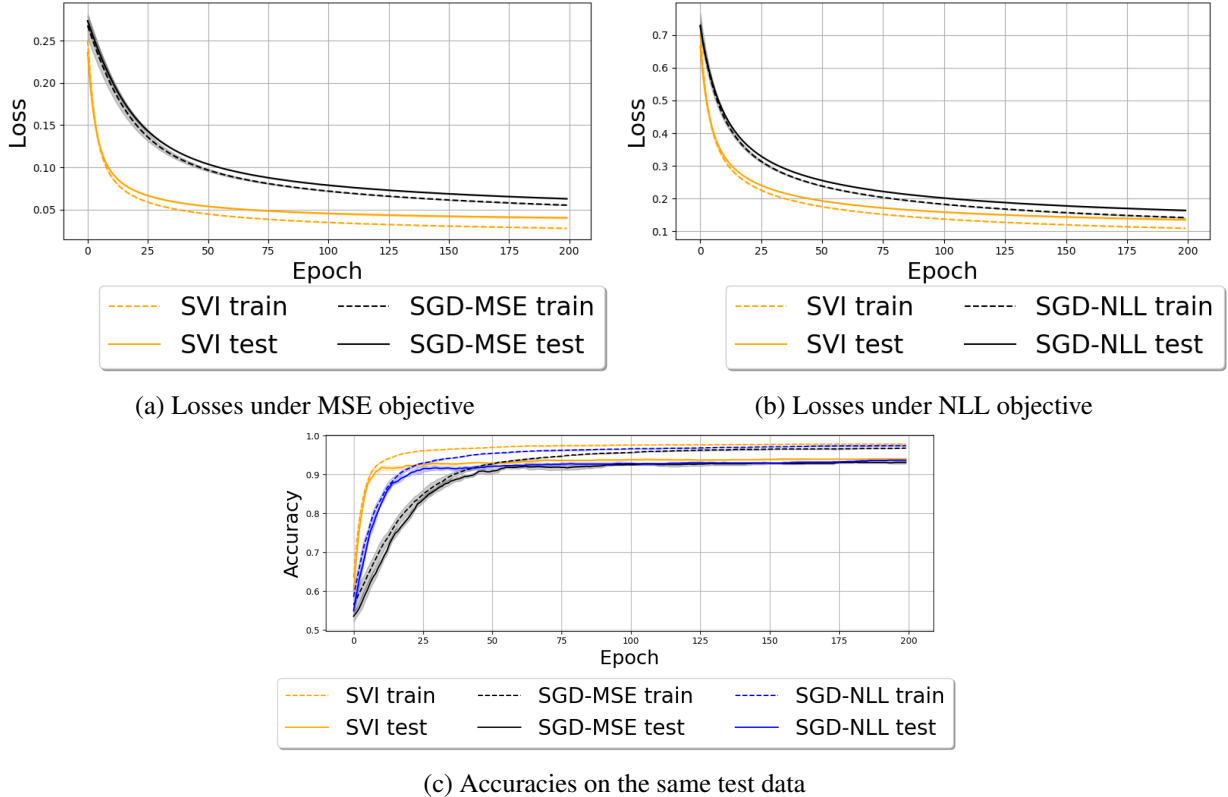


Figure 3: One-layer fully-connected network. In (a) and (b), we plot training and test losses for both SGD (black) and SVI (orange). The loss choice for SGD is the mean-squared error (MSE) in (a) and the negative log-likelihood (NLL) in (b). The SVI update for one-layer training is based on sample version of (3), which does not depend on the loss objective; thus, we compute the MSE or NLL losses for SVI for comparison. In (c), we show the binary classification accuracies by SVI in orange, SGD by MSE (SGD-MSE) in black, and SGD by NLL (SGD-NLL) in blue.

In addition, all results are averaged over three random trials, where networks are re-initialized in each trial. In simulation, we also redraw training samples in each trial. We show standard errors in tables as brackets and plots as error bars.

Notation-wise, $X \sim \mathcal{N}(a, b)$ means the random variable X follows a normal distribution with mean a and variance b^2 ; N (resp. N_1) denotes the size of training (resp. test) sample, lr denotes the learning rate, B denotes the batch size, and E denotes training epochs.

6.3 Synthetic data experiments

6.3.1 One-layer network training

We first consider data generated from a one-layer probit model, which leads to non-convex objectives. Specifically, for each $i \geq 1$, let $X^{(i)} \in \mathbb{R}^p$, $Y^{(i)} \in \{0, 1\}$ and

$$\mathbb{E}[Y^{(i)}|X^{(i)}] = \Phi(\beta^T X^{(i)} + b),$$

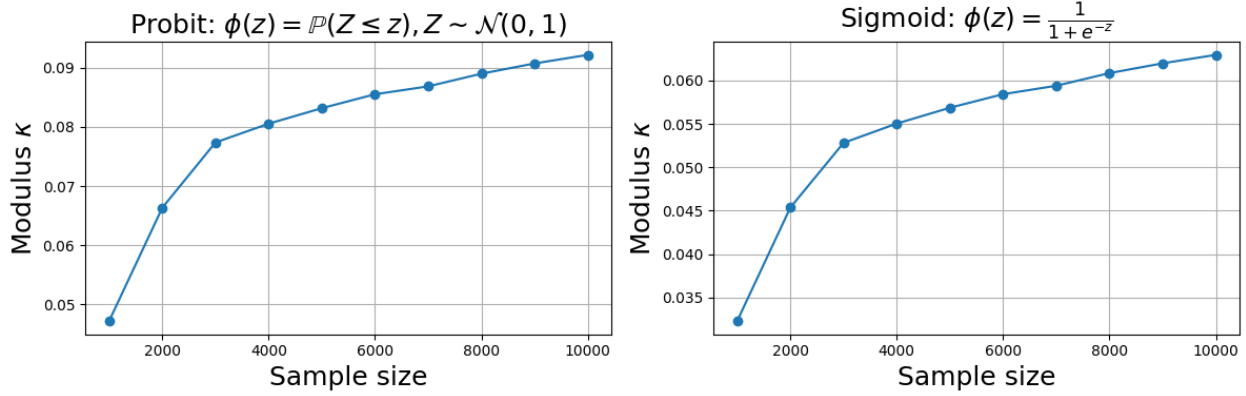


Figure 4: Modulus κ evaluated on training data for the one-layer network training in Section 6.3.1. We vary the activation function ϕ and plot the corresponding κ values over increasing number of training samples.

where $\Phi(z) = \mathbb{P}(Z \leq z)$ for $Z \sim \mathcal{N}(0, 1)$. Let the subscript j denotes the j -th entry. We then sample $X_j^{(i)} \stackrel{i.i.d.}{\sim} \mathcal{N}(0.05, 1)$, $\beta_j \stackrel{i.i.d.}{\sim} \mathcal{N}(-0.05, 1)$, and $b \sim \mathcal{N}(-0.1, 1)$. We let $N = 2000$, $N_1 = 500$, and use a fully-connected one-layer network. We further let $B = 200$ and $E = 200$ and use $\text{lr} = 0.005$.

To train SVI and SGD, we use both the MSE objective and the negative log-likelihood (NLL) objectives. Note that in this one-layer setting, SVI provides monotone operators as parameter update directions that are independent of the training objective (recall the definition in (3)). Figure 3 shows the training and test performances by both methods. On test data, SVI consistently yields smaller losses and higher prediction accuracies than SGD under both MSE and NLL objectives during training. This shows the effectiveness of SVI in cases with theoretical guarantees. Figure 4 additionally visualizes the modulus κ as a function of the sample size, where we see κ is always positive (so the operator is strongly monotone) and increases as sample sizes grow.

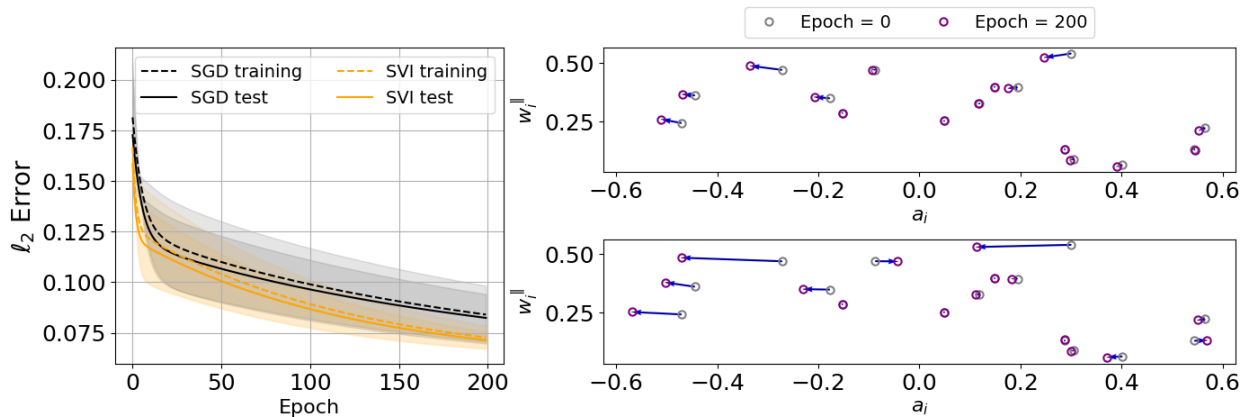


Figure 5: Two-layer GNN prediction error and neuron dynamics visualization. Left: ℓ_2 error in (17). Right: visualization of the training dynamics by SGD (top) and SVI (bottom).

Table 1: Two-layer GNN model on random graphs with an increasing number of graph nodes. We show the training and test ℓ_2 error as defined in (17) along the training epochs. Entries in brackets indicate standard deviation over 3 independent initialization of model parameters.

(a) Epoch 50					(b) Epoch 100				
# nodes	SGD train	SVI train	SGD test	SVI test	# nodes	SGD train	SVI train	SGD test	SVI test
15	0.110 (2.01e-2)	0.104 (1.72e-2)	0.107 (1.63e-2)	0.101 (1.34e-2)	15	0.099 (1.79e-2)	0.089 (1.21e-2)	0.097 (1.46e-2)	0.087 (9.09e-3)
40	0.102 (1.60e-2)	0.096 (1.39e-2)	0.101 (1.60e-2)	0.095 (1.38e-2)	40	0.092 (1.45e-2)	0.083 (1.04e-2)	0.092 (1.47e-2)	0.083 (1.05e-2)
100	0.092 (1.27e-2)	0.087 (1.13e-2)	0.093 (1.37e-2)	0.088 (1.22e-2)	100	0.085 (1.18e-2)	0.078 (9.29e-3)	0.086 (1.30e-2)	0.079 (1.03e-2)
300	0.080 (9.48e-3)	0.077 (8.80e-3)	0.081 (1.04e-2)	0.077 (9.68e-3)	300	0.076 (9.09e-3)	0.070 (7.86e-3)	0.077 (1.01e-2)	0.071 (8.78e-3)
600	0.073 (7.63e-3)	0.070 (7.34e-3)	0.074 (8.32e-3)	0.071 (7.98e-3)	600	0.070 (7.43e-3)	0.064 (6.86e-3)	0.070 (8.14e-3)	0.065 (7.54e-3)

(c) Epoch 200				
# nodes	SGD train	SVI train	SGD test	SVI test
15	0.084 (1.43e-2)	0.073 (5.81e-3)	0.082 (1.17e-2)	0.071 (4.11e-3)
40	0.079 (1.21e-2)	0.069 (5.76e-3)	0.079 (1.26e-2)	0.068 (6.20e-3)
100	0.075 (1.06e-2)	0.066 (6.55e-3)	0.077 (1.19e-2)	0.067 (7.75e-3)
300	0.069 (8.61e-3)	0.060 (6.50e-3)	0.070 (9.67e-3)	0.061 (7.49e-3)
600	0.064 (7.23e-3)	0.056 (6.05e-3)	0.065 (7.97e-3)	0.056 (6.80e-3)

6.3.2 Two-layer GNN training

Table 1 shows that SVI consistently reaches smaller ℓ_2 prediction error for the two-layer GNN, even when the graph is large (600 nodes). This shows the robustness of the proposed SVI, even in this setting beyond our theoretical analyses. To better understand how SVI update parameters, Fig. 5 zooms in the dynamics for 16 neurons (right figure) and shows the corresponding ℓ_2 model recovery test error (left figure). Regarding the right figure, we plot the norm of first-layer neuron weights, where the norm is defined in terms of the inner product with initial weights, against the second-layer neuron weights, which are scalars because $k = 1$. One circle represents one neuron, with arrows representing the direction of moving along the initial weights. We then connect the initial and final dots to indicate the displacement of neurons. The same visualization techniques are used in [Pellegrini and Biroli, 2020]. We observe that SVI displaces neurons further after 200 epochs, which is anticipated in Remark 5.1. In this case, it can be beneficial due to the faster error convergence.

6.4 Real-data network prediction

For real-data experiments, we use larger networks (i.e., three layers or more). Examples include spatial-temporal anomaly detection on network data, graph nodal classification on large graphs, and image

Table 2: Solar ramping event detection under varying sizes of the GNN. Entries in brackets indicate standard deviation over three independent initializations of model parameters.

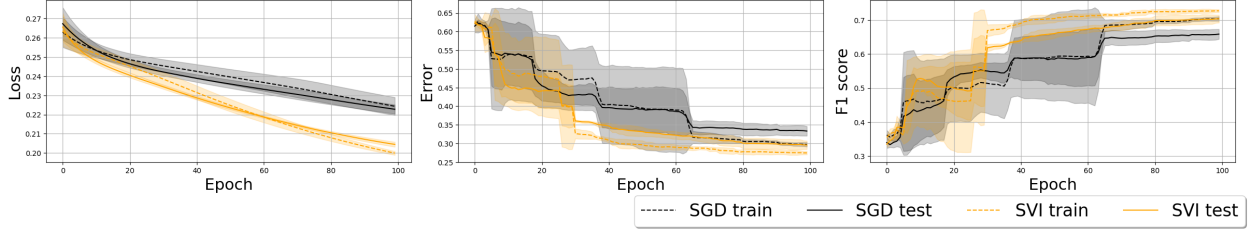
(a) MSE loss					(b) Classification error				
# hidden neurons	SGD Training	SVI Training	SGD Test	SVI Test	# hidden neurons	SGD Training	SVI Training	SGD Test	SVI Test
32	0.224 (4.67e-3)	0.200 (9.95e-4)	0.223 (2.40e-3)	0.204 (1.30e-3)	32	0.297 (5.88e-3)	0.275 (4.54e-3)	0.333 (1.28e-2)	0.296 (1.13e-2)
64	0.213 (7.66e-4)	0.191 (8.49e-4)	0.211 (1.67e-3)	0.195 (1.12e-3)	64	0.283 (4.33e-3)	0.263 (1.59e-3)	0.308 (1.04e-2)	0.272 (1.15e-3)
128	0.219 (1.79e-3)	0.195 (6.22e-4)	0.217 (1.13e-3)	0.199 (5.14e-4)	128	0.295 (3.15e-3)	0.267 (2.43e-3)	0.328 (6.13e-3)	0.282 (9.04e-4)

(c) Weighted F_1 score				
# hidden neurons	SGD Training	SVI Training	SGD Test	SVI Test
32	0.704 (6.62e-3)	0.727 (4.36e-3)	0.659 (1.46e-2)	0.704 (1.15e-2)
64	0.719 (4.57e-3)	0.737 (1.59e-3)	0.689 (1.16e-2)	0.728 (1.14e-3)
128	0.706 (3.50e-3)	0.734 (2.41e-3)	0.664 (7.73e-3)	0.718 (9.11e-4)

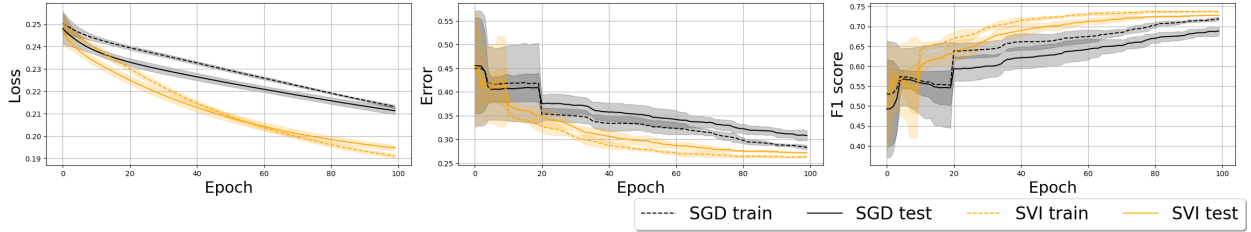
Table 3: Traffic data multi-class anomaly detection under varying sizes of the GNN. Entries in brackets indicate standard deviation over three independent initializations of model parameters.

(a) MSE loss					(b) Classification error				
# hidden neurons	SGD Training	SVI Training	SGD Test	SVI Test	# hidden neurons	SGD Training	SVI Training	SGD Test	SVI Test
32	0.529 (2.84e-2)	0.475 (7.64e-3)	0.529 (2.51e-2)	0.477 (5.63e-3)	32	0.401 (2.49e-2)	0.367 (1.24e-2)	0.404 (2.22e-2)	0.371 (9.59e-3)
64	0.471 (8.25e-3)	0.457 (6.51e-3)	0.473 (7.67e-3)	0.458 (5.19e-3)	64	0.344 (9.52e-3)	0.339 (5.86e-3)	0.349 (1.12e-2)	0.345 (6.66e-3)
128	0.447 (2.70e-3)	0.445 (1.84e-3)	0.448 (2.44e-3)	0.445 (1.98e-3)	128	0.334 (1.64e-3)	0.334 (2.00e-3)	0.335 (2.03e-3)	0.334 (3.27e-3)

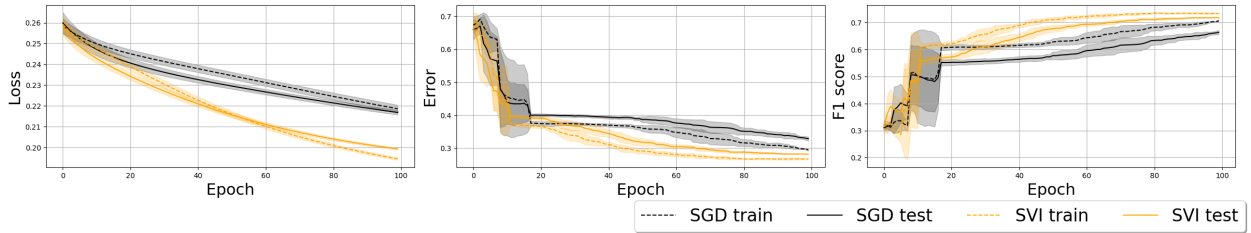
(c) Weighted F_1 score				
# hidden neurons	SGD Training	SVI Training	SGD Test	SVI Test
32	0.594 (2.89e-2)	0.629 (1.67e-2)	0.589 (2.76e-2)	0.626 (1.29e-2)
64	0.655 (9.91e-3)	0.660 (6.05e-3)	0.651 (1.14e-2)	0.655 (6.71e-3)
128	0.665 (1.77e-3)	0.665 (1.97e-3)	0.664 (2.16e-3)	0.666 (3.36e-3)



(a) 32 hidden neurons. Left to right: MSE loss, classification error, and weighted F_1 score.



(b) 64 hidden neurons. Left to right: MSE loss, classification error, and weighted F_1 score.



(c) 128 hidden neurons. Left to right: MSE loss, classification error, and weighted F_1 score.

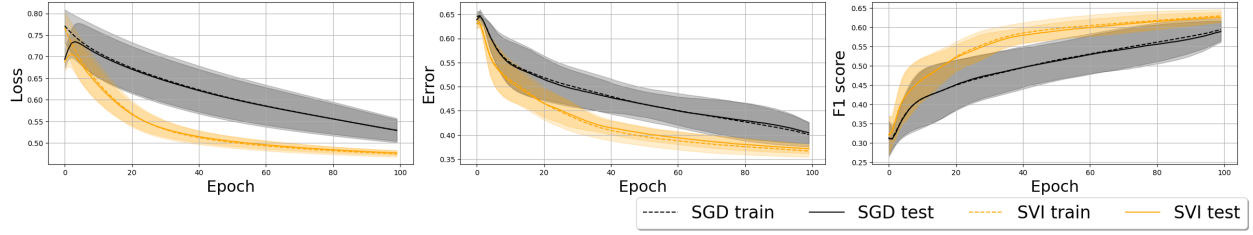
Figure 6: Solar ramping event detection under various hidden neurons. Results are plotted with one standard error bars over three independent trials.

classification. The output layer uses sigmoid (binary classification) or softmax (multi-class classification).

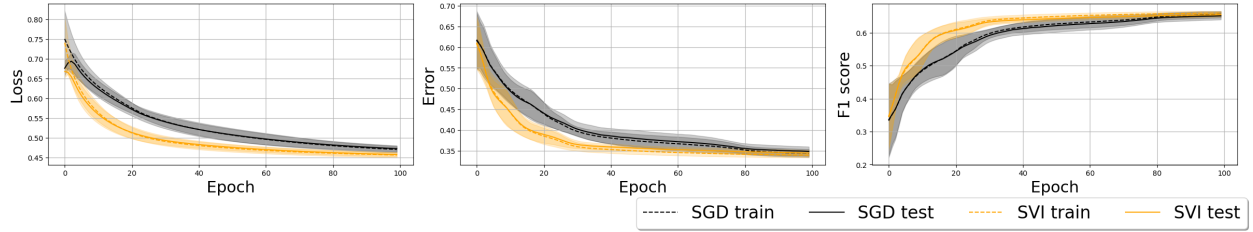
6.4.1 Binary solar ramping prediction

The raw solar radiation data are retrieved from the National Solar Radiation Database for 2017 and 2018. We consider data from 10 cities downtown in California and from 9 locations in downtown Los Angeles, where each city or location is a node in the network. In this experiment, the goal is to identify ramping events within a network of solar sensors, where ramping events are defined over abrupt changes in the sensor inputs. Thus, $Y^{(i)} = 1$ if node i at day t experiences a ramping event. We define feature $X^{(i)}$ as the collection of past d days of observation and pick $d = 5$. We estimate edges via a k -nearest neighbor approach based on the correlation between training ramping labels, with $k = 4$. Data in 2017 are used for training ($N = 360$) and the rest for testing ($N_1 = 365$), and we let $B = 30$, $E = 100$, and $\text{lr} = 0.001$.

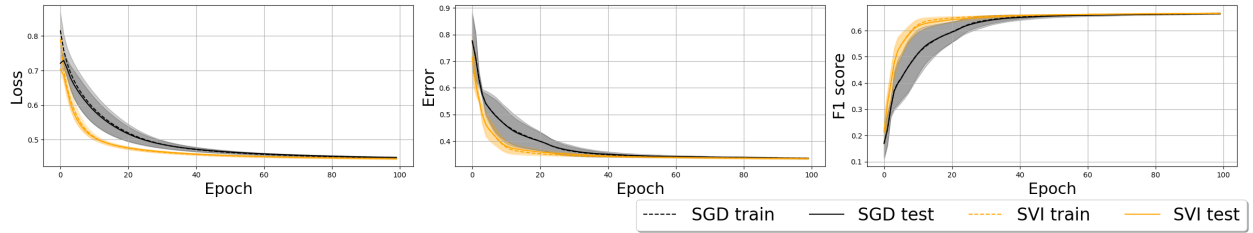
Table 2 shows that under varying numbers of hidden nodes in the GNN, SVI consistently reaches lower test classification error and higher test weighted F_1 scores; the F_1 scores are weighted by support (the number of true instances for each label). Figure 6 shows faster intermediate convergence results by SVI in terms of both metrics.



(a) 32 hidden neurons. Left to right: MSE loss, classification error, and weighted F_1 score.



(b) 64 hidden neurons. Left to right: MSE loss, classification error, and weighted F_1 score.



(c) 128 hidden neurons. Left to right: MSE loss, classification error, and weighted F_1 score.

Figure 7: Traffic data multi-class anomaly detection under various hidden neurons. Results are plotted with one standard error bar over three independent trials.

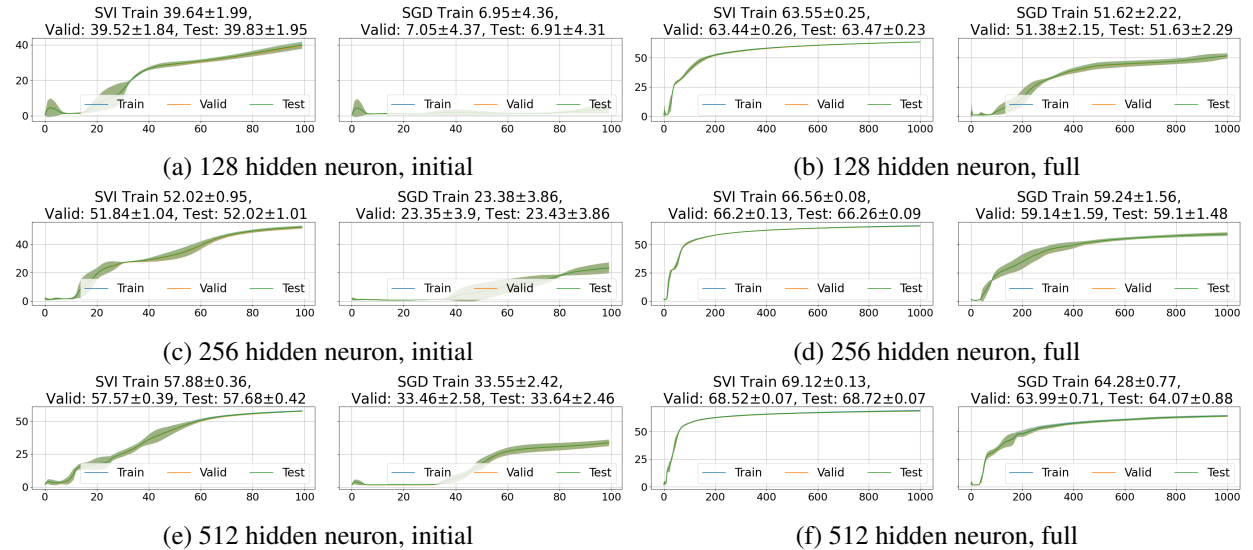


Figure 8: Classification accuracies on the large-scale ogbn-arxiv dataset. We visualize the prediction accuracies during the initial (i.e., 100 epochs) and full (i.e., 1000 epochs) training stages.

6.4.2 Multi-class traffic flow anomaly detection

The raw bi-hourly traffic flow data are from the California Department of Transportation, where we collected data from 20 non-uniformly spaced traffic sensors in 2020. This experiment aims to identify multi-class bi-hourly anomalous traffic flow observations in a sensor network. Thus, we let $Y^{(i)} = 1$ (resp. 2) if the current traffic flow lies outside the upper (resp. lower) 90% quantile over the past four days of traffic flow of its nearest four neighbors based on sensor proximity. As before, we define feature $X^{(i)}$ as the collection of past d days of observation and set $d = 4$, where the edges include the nearest five neighbors based on location. Data in the first nine months are training data (e.g., $N = 6138$) and the rest for testing ($N_1 = 2617$). We let $B = 600$, $E = 100$, and $\text{lr} = 0.001$.

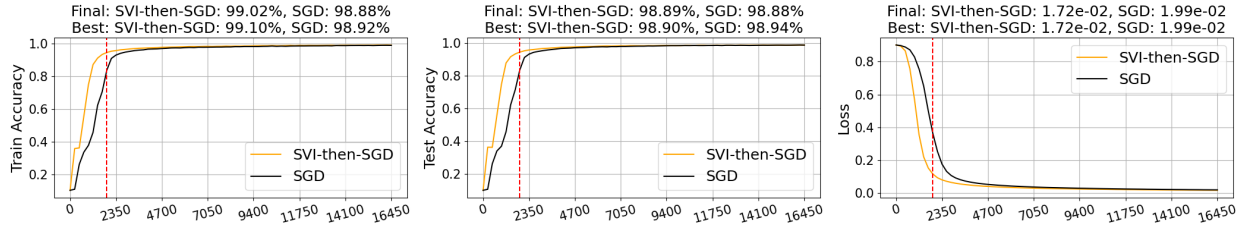
Table 3 shows that SVI consistently reaches lower test classification error and higher test weighted F_1 scores. This is consistent with the previous observations and holds with varying sizes of the GNN. Figure 7 shows faster intermediate convergence results by SVI in terms of both metrics.

6.4.3 Multi-class large-scale OGB node classification

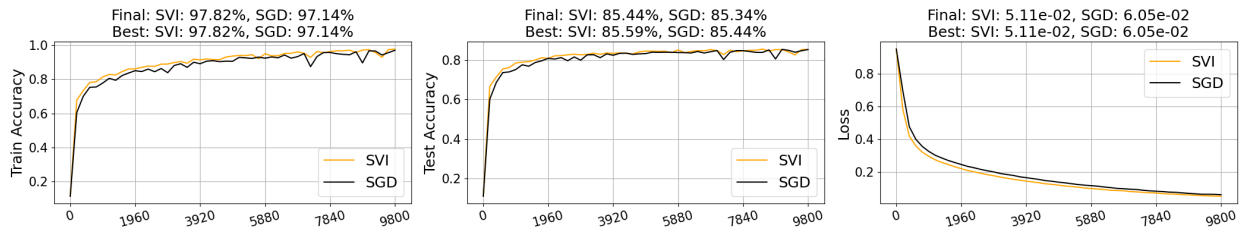
We further demonstrate the applicability of SVI on the large `ogbn-arxiv` graph provided by the Open Graph Benchmark (OGB) [Hu et al., 2020, 2021]. The graph is much larger than earlier examples: graph nodes are papers to be classified, and edges denote citation among papers; it has approximately 170 thousand nodes, 1.16 million edges, 128-dimensional node features, and 40 node classes. These numbers are significantly larger than those in earlier examples. We train four-layer GNN models with varying numbers of hidden nodes, where these GNN models are wider and deeper than the earlier ones we trained. We train for

Table 4: Classification accuracies on the large `ogbn-arxiv` dataset under varying sizes of the GNN. “Initial” (resp. “Final”) results indicate prediction accuracies after training 100 (resp. 1000) epochs. Entries in brackets show standard deviation over three independent trials.

# hidden neurons	result type	SVI			SGD		
		Train	Valid	Test	Train	Valid	Test
128	Initial	39.64 (1.99)	39.52 (1.84)	39.83 (1.95)	6.95 (4.36)	7.05 (4.37)	6.91 (4.31)
	Final	63.55 (0.25)	63.44 (0.26)	63.47 (0.23)	51.62 (2.22)	51.38 (2.15)	51.63 (2.29)
256	Initial	52.02 (0.95)	51.84 (1.04)	52.02 (1.01)	23.38 (3.86)	23.35 (3.9)	23.43 (3.86)
	Final	66.56 (0.08)	66.2 (0.13)	66.26 (0.09)	59.24 (1.56)	59.14 (1.59)	59.1 (1.48)
512	Initial	57.88 (0.36)	57.57 (0.39)	57.68 (0.42)	33.55 (2.42)	33.46 (2.58)	33.64 (2.46)
	Final	69.12 (0.13)	68.52 (0.07)	68.72 (0.07)	64.28 (0.77)	63.99 (0.71)	64.07 (0.88)



(a) MNIST by LeNet: training accuracy (left), test accuracy (middle), and training loss (right).



(b) CIFAR10 by VGG-16: training accuracy (left), test accuracy (middle), and training loss (right).

Figure 9: Classification accuracies and training losses by both methods. We plot the metrics over training batches in each sub-figure. In the title, “Final” represents the metric at the end of all training epochs, and “Best” represents the highest/lowest metric throughout training epochs. On MNIST, training before the dashed-dotted red line is by *SVI*, and we continue to train the *SVI*-warm-started model afterward by *SGD* to reach the optimal performance.

fixed $E = 1000$ epochs where B equals all training nodes. The learning rate $lr = 0.001$.

Table 4 compares *SVI* against *SGD* under various network sizes. We see that *SVI* consistently reaches higher initial and final classification accuracies on training, validation, and test data. Figure 8 shows the convergence of prediction accuracy along training epochs, where *SVI* consistently remains higher in terms of prediction accuracies along training epochs. We believe such faster convergence can benefit large-scale experiments, where it is computationally demanding to run many training epochs.

6.4.4 Image classification datasets

We compare *SVI* with the gradient-based method on training image classifiers on the MNIST dataset [LeCun, 1998] and the CIFAR-10 dataset [Krizhevsky et al., 2009]. On MNIST, we train the LeNet [LeCun et al., 1998] model, which consists of two convolutional layers as image feature extractors, followed by prediction with three fully-connected layers. On CIFAR10, we train the VGG-16 model [Simonyan and Zisserman, 2015], which has 16 convolutional layers. The lr is fixed as 0.005 throughout training, and we fix the batch size B to be 128.

Figure 9 shows training and test metrics over training batches. Note that on MNIST, we train the initial 10% of total training batches by *SVI* and the rest 90% by *SGD*, and we call this hybrid technique *SVI-then-SGD*. We do so because *SVI* shows fast initial convergence, yet to reach the optimal performance after the initial stages, gradient-based methods can be more desirable. On MNIST, the hybrid approach shows faster initial convergence than *SGD* due to the use of *SVI* and reaches higher accuracy and lower loss by the end of

all training batches. On CIFAR-10, the performance of SVI is also competitive.

7 Conclusion

We have investigated how a new monotone VI approach can be useful in training neural networks, with prediction guarantees for last-layer fine-tuning and competitive performance as SGD. We specifically provide theoretical justifications when training parameters in the last layer, assuming previous layers are frozen. On various synthetic and real-data examples, our SVI improves efficiency in the early stage of training and reaches competitive/better final performance as SGD.

The work can be extended in several directions. Testing the performance of SVI on training large models with high-dimensional data is important. Theoretically, we wish to extend the analyses to multi-layer network training. Application-wise, addressing a broader range of problems in GNN is helpful, including edge and graph classification [Zhou et al., 2020] and various regression problems.

Acknowledgements

This work is partially supported by an NSF CAREER CCF-1650913, NSF DMS-2134037, CMMI-2015787, CMMI-2112533, DMS-1938106, DMS-1830210, and the Coca-Cola Foundation. XC is also partially supported by NSF DMS-2237842 and Simons Foundation.

References

- Zeyuan Allen-Zhu, Yuanzhi Li, and Zhao Song. A convergence theory for deep learning via overparameterization. In *International Conference on Machine Learning*, pages 242–252. PMLR, 2019.
- Ehsan Amid, Rohan Anil, and Manfred Warmuth. Locoprop: Enhancing backprop via local loss optimization. In *International Conference on Artificial Intelligence and Statistics*, pages 9626–9642. PMLR, 2022.
- Sanjeev Arora, Simon Du, Wei Hu, Zhiyuan Li, and Ruosong Wang. Fine-grained analysis of optimization and generalization for overparameterized two-layer neural networks. In *International Conference on Machine Learning*, pages 322–332. PMLR, 2019a.
- Sanjeev Arora, Simon S Du, Wei Hu, Zhiyuan Li, Russ R Salakhutdinov, and Ruosong Wang. On exact computation with an infinitely wide neural net. In *Advances in Neural Information Processing Systems*, pages 8139–8148, 2019b.
- Patrick L. Combettes, Jean-Christophe Pesquet, and Audrey Repetti. A variational inequality model for learning neural networks. In *ICASSP 2023 - 2023 IEEE International Conference on Acoustics, Speech and Signal Processing (ICASSP)*, pages 1–5, 2023. doi: 10.1109/ICASSP49357.2023.10095688.

- Michaël Defferrard, Xavier Bresson, and Pierre Vandergheynst. Convolutional neural networks on graphs with fast localized spectral filtering. *Advances in neural information processing systems*, 29:3844–3852, 2016.
- Ning Ding, Yujia Qin, Guang Yang, Fuchao Wei, Zonghan Yang, Yusheng Su, Shengding Hu, Yulin Chen, Chi-Min Chan, Weize Chen, et al. Parameter-efficient fine-tuning of large-scale pre-trained language models. *Nature Machine Intelligence*, 5(3):220–235, 2023.
- Simon Du, Jason Lee, Haochuan Li, Liwei Wang, and Xiyu Zhai. Gradient descent finds global minima of deep neural networks. In *International Conference on Machine Learning*, pages 1675–1685. PMLR, 2019.
- John C. Duchi, Elad Hazan, and Yoram Singer. Adaptive subgradient methods for online learning and stochastic optimization. In *J. Mach. Learn. Res.*, 2010.
- Francisco Facchinei and Jong-Shi Pang. *Finite-dimensional variational inequalities and complementarity problems*. Springer, 2003.
- Matthias Fey and Jan E. Lenssen. Fast graph representation learning with PyTorch Geometric. In *ICLR Workshop on Representation Learning on Graphs and Manifolds*, 2019.
- Bolin Gao and Lacra Pavel. On the properties of the softmax function with application in game theory and reinforcement learning, 2018.
- William L Hamilton, Rex Ying, and Jure Leskovec. Inductive representation learning on large graphs. In *Proceedings of the 31st International Conference on Neural Information Processing Systems*, pages 1025–1035, 2017.
- Weihua Hu, Matthias Fey, Marinka Zitnik, Yuxiao Dong, Hongyu Ren, Bowen Liu, Michele Catasta, and Jure Leskovec. Open graph benchmark: Datasets for machine learning on graphs. *Advances in neural information processing systems*, 33:22118–22133, 2020.
- Weihua Hu, Matthias Fey, Hongyu Ren, Maho Nakata, Yuxiao Dong, and Jure Leskovec. Ogb-lsc: A large-scale challenge for machine learning on graphs. In *Thirty-fifth Conference on Neural Information Processing Systems Datasets and Benchmarks Track (Round 2)*, 2021.
- Sergey Ioffe and Christian Szegedy. Batch normalization: Accelerating deep network training by reducing internal covariate shift. In *International conference on machine learning*, pages 448–456. pmlr, 2015.
- Anatoli Juditsky and Arkadi Nemirovski. On well-structured convex–concave saddle point problems and variational inequalities with monotone operators. *Optimization Methods and Software*, 37(5):1567–1602, 2022.
- Anatoli B. Juditsky and Arkadi S. Nemirovsky. Signal recovery by stochastic optimization. *Autom. Remote. Control.*, 80:1878–1893, 2019.

- David Kinderlehrer and Guido Stampacchia. *An introduction to variational inequalities and their applications*. SIAM, 2000.
- DP Kingma. Adam: a method for stochastic optimization. In *Int Conf Learn Represent*, 2014.
- Thomas N. Kipf and Max Welling. Semi-supervised classification with graph convolutional networks. In *5th International Conference on Learning Representations, ICLR 2017, Toulon, France, April 24-26, 2017, Conference Track Proceedings*. OpenReview.net, 2017.
- Georgios Kotsalis, Guanghui Lan, and Tianjiao Li. Simple and optimal methods for stochastic variational inequalities, i: operator extrapolation. *SIAM Journal on Optimization*, 32(3):2041–2073, 2022.
- Alex Krizhevsky, Geoffrey Hinton, et al. Learning multiple layers of features from tiny images. 2009.
- Yann LeCun. The mnist database of handwritten digits. <http://yann.lecun.com/exdb/mnist/>, 1998.
- Yann LeCun, Léon Bottou, Yoshua Bengio, and Patrick Haffner. Gradient-based learning applied to document recognition. *Proceedings of the IEEE*, 86(11):2278–2324, 1998.
- Haokun Liu, Derek Tam, Mohammed Muqeeth, Jay Mohta, Tenghao Huang, Mohit Bansal, and Colin A Raffel. Few-shot parameter-efficient fine-tuning is better and cheaper than in-context learning. *Advances in Neural Information Processing Systems*, 35:1950–1965, 2022.
- Mingrui Liu, Hassan Rafique, Qihang Lin, and Tianbao Yang. First-order convergence theory for weakly-convex-weakly-concave min-max problems. *Journal of Machine Learning Research*, 22(169):1–34, 2021.
- Song Mei, Andrea Montanari, and Phan-Minh Nguyen. A mean field view of the landscape of two-layer neural networks. *Proceedings of the National Academy of Sciences*, 115(33):E7665–E7671, 2018.
- Behnam Neyshabur, Ryota Tomioka, and Nathan Srebro. In search of the real inductive bias: On the role of implicit regularization in deep learning. In *International Conference on Learning Representations (ICLR) workshop track*, 2014.
- Jiri Outrata, Michal Kocvara, and Jochem Zowe. *Nonsmooth approach to optimization problems with equilibrium constraints: theory, applications and numerical results*, volume 28. Springer Science & Business Media, 2013.
- Adam Paszke, Sam Gross, Soumith Chintala, Gregory Chanan, Edward Yang, Zachary DeVito, Zeming Lin, Alban Desmaison, Luca Antiga, and Adam Lerer. Automatic differentiation in pytorch. In *NIPS 2017 Workshop Autodiff*, 2017.
- Adam Paszke, Sam Gross, Francisco Massa, Adam Lerer, James Bradbury, Gregory Chanan, Trevor Killeen, Zeming Lin, Natalia Gimelshein, Luca Antiga, Alban Desmaison, Andreas Kopf, Edward Yang, Zachary DeVito, Martin Raison, Alykhan Tejani, Sasank Chilamkurthy, Benoit Steiner, Lu Fang, Junjie Bai, and Soumith Chintala. Pytorch: An imperative style, high-performance deep learning library. In H. Wallach,

H. Larochelle, A. Beygelzimer, F. d'Alché-Buc, E. Fox, and R. Garnett, editors, *Advances in Neural Information Processing Systems 32*, pages 8024–8035. Curran Associates, Inc., 2019.

Franco Pellegrini and Giulio Biroli. An analytic theory of shallow networks dynamics for hinge loss classification. *Advances in Neural Information Processing Systems*, 33:5356–5367, 2020.

Mert Pilanci and Tolga Ergen. Neural networks are convex regularizers: Exact polynomial-time convex optimization formulations for two-layer networks. In *ICML*, 2020.

Karen Simonyan and Andrew Zisserman. Very deep convolutional networks for large-scale image recognition. In Yoshua Bengio and Yann LeCun, editors, *3rd International Conference on Learning Representations, ICLR 2015, San Diego, CA, USA, May 7-9, 2015, Conference Track Proceedings*, 2015.

Ilya Sutskever, James Martens, George Dahl, and Geoffrey Hinton. On the importance of initialization and momentum in deep learning. In Sanjoy Dasgupta and David McAllester, editors, *Proceedings of the 30th International Conference on Machine Learning*, volume 28 of *Proceedings of Machine Learning Research*, pages 1139–1147, Atlanta, Georgia, USA, 17–19 Jun 2013. PMLR.

Zonghan Wu, Shirui Pan, Fengwen Chen, Guodong Long, Chengqi Zhang, and Philip S. Yu. A comprehensive survey on graph neural networks. *IEEE Transactions on Neural Networks and Learning Systems*, 32:4–24, 2019.

Jie Zhou, Ganqu Cui, Shengding Hu, Zhengyan Zhang, Cheng Yang, Zhiyuan Liu, Lifeng Wang, Changcheng Li, and Maosong Sun. Graph neural networks: A review of methods and applications. *AI open*, 1:57–81, 2020.

A Proofs

Proof of Lemma 4.1. We first verify the monotonicity of F by considering vectorized parameters, where for a matrix $A \in \mathbb{R}^{m \times n}$, $\text{vec}(A) \in \mathbb{R}^{mn}$ by stacking vertically columns of A . Note that this vectorization is simply used to make sure the Euclidean inner product between F and θ_L is well-defined; the fundamental meaning of θ_L (e.g., as the channel-mixing coefficient) remains unchanged. With an abuse of notation, we use the same θ_L and Θ to denote the vectorized parameter and the corresponding parameter space. For any $\theta_{1,L}, \theta_{2,L} \in \Theta$,

$$\begin{aligned}
& \langle F(\theta_{1,L}) - F(\theta_{2,L}), \theta_{1,L} - \theta_{2,L} \rangle \\
&= \langle \mathbb{E}_X \{ \eta^*(X)^\top (\phi_L(\eta^*(X)\theta_{1,L}) - \phi_L(\eta^*(X)\theta_{2,L})) \}, \theta_{1,L} - \theta_{2,L} \rangle \\
&= \mathbb{E}_X \{ (\phi_L(\eta^*(X)\theta_{1,L}) - \phi_L(\eta^*(X)\theta_{2,L}))^\top (\eta^*(X)\theta_{1,L} - \eta^*(X)\theta_{2,L}) \} \\
&\geq \lambda_{\min}(\nabla \phi_L) \mathbb{E}_X \{ \|\eta^*(X)\theta_{1,L} - \eta^*(X)\theta_{2,L}\|_2^2 \} \\
&\geq \underbrace{\lambda_{\min}(\nabla \phi_L) \lambda_{\min}(\mathbb{E}_X \{ \eta^*(X)^\top \eta^*(X) \})}_{\kappa} \|\theta_{1,L} - \theta_{2,L}\|_2^2,
\end{aligned}$$

where κ is defined in (2). The first equality uses the fact that the Y part is cancelled and the first inequality holds when ϕ_L is *continuously differentiable* on its domain.

We then verify the K_2 -Lipschitz continuity of F . For any $\theta_{1,L}, \theta_{2,L} \in \Theta$,

$$\begin{aligned} \|F(\theta_{1,L}) - F(\theta_{2,L})\|_2 &= \mathbb{E}_X \{ \|\eta^*(X)^\top (\phi_L(\eta^*(X)\theta_{1,L}) - \phi_L(\eta^*(X)\theta_{2,L}))\|_2 \} \\ &\leq \mathbb{E}_X \{ \|\eta^*(X)^\top\|_2 \|\phi_L(\eta^*(X)\theta_{1,L}) - \phi_L(\eta^*(X)\theta_{2,L})\|_2 \} \\ &\leq K \mathbb{E}_X \{ \|\eta^*(X)\|_2 \|\eta^*(X)\theta_{1,L} - \eta^*(X)\theta_{2,L}\|_2 \} \\ &\leq \underbrace{K \mathbb{E}_X \{ \|\eta^*(X)\|_2^2 \}}_{K_2} \|\theta_{1,L} - \theta_{2,L}\|_2^2, \end{aligned}$$

where K_2 has been defined. We repeated used the Cauchy–Schwarz inequality and the last inequality relies on the assumption that ϕ_L is K -Lipschitz continuous.

Note that given random samples $\{X_1, \dots, X_N\}$, the quantities $\lambda_{\min}(\mathbb{E}_X \{ \eta^*(X)^\top \eta^*(X) \})$ and $\mathbb{E}_X \{ \|\eta^*(X)\|_2^2 \}$ can be empirically approximated by sample averages. Thus, under θ_L^* ,

$$\begin{aligned} F(\theta_L^*) &= \mathbb{E}_{X,Y} \{ \eta^\top [\phi_L(\eta^*(X)\theta_L^*) - Y] \} \\ &= \mathbb{E}_{X,Y} \{ \eta^*(X)^\top [\phi_L(\eta^*(X)\theta_L^*) - \phi_L(\eta^*(X)\theta_L^*)] \} = 0, \end{aligned}$$

where we used the fact that $\mathbb{E}[Y|X] = \phi_L(\eta^*(X)\theta_L^*)$.

□

Proof of Lemma 4.2. The proof employs classical techniques when analyzing the convergence of projection descent in stochastic optimization, which appear in [Juditsky and Nemirovsky, 2019, Proposition 3.2].

First, for any $\theta_L \in \Theta$,

$$\begin{aligned} \mathbb{E}_{(X,Y(\theta_L))} \{ \|\eta^*(X)^\top \phi_L(\eta^*(X)\theta_L)\|_2 \} &= \mathbb{E}_X \{ \|\mathbb{E}_{Y(\theta_L)} \{ \eta^*(X)Y(\theta_L) \}\|_2 \} \\ &\leq \mathbb{E}_X \mathbb{E}_{Y(\theta_L)} \{ \|\eta^*(X)Y(\theta_L)\|_2 \} \quad [\text{Jensen's Inequality}] \\ &= \mathbb{E}_{(X,Y(\theta_L))} \{ \|\eta^*(X)Y(\theta_L)\|_2 \} \leq M. \end{aligned}$$

By the form of F , we then have that $\mathbb{E}_{X,Y} \{ \|F(\theta_L)\|_2^2 \} \leq 4M^2$ for any θ_L .

Next, note that each $\hat{\theta}_L^{(t)}$ is a deterministic function of \mathcal{D}^{Tr} . Define the difference of estimation and its expected value as

$$D_t(\mathcal{D}^{\text{Tr}}) = \frac{1}{2} \|\hat{\theta}_L^{(t)} - \theta_L^*\|_2^2, \quad d_t = \mathbb{E}_{\mathcal{D}^{\text{Tr}}} \{ D_t(\mathcal{D}^{\text{Tr}}) \}.$$

As a result,

$$\begin{aligned}
D_t(\mathcal{D}^{\text{Tr}}) &= \frac{1}{2} \|\text{Proj}_\Theta \left[\hat{\theta}_L^{(t-1)} - \gamma_t \widehat{F}^T(\hat{\theta}_L^{(t-1)}) - \theta_L^* \right]\|_2^2 \\
&\leq \frac{1}{2} \|\hat{\theta}_L^{(t-1)} - \gamma_t \widehat{F}^T(\hat{\theta}_L^{(t-1)}) - \theta_L^*\|_2^2 \quad [\text{The projection is a contraction}] \\
&= \frac{1}{2} \|\hat{\theta}_L^{(t-1)} - \theta_L^*\|_2^2 - \gamma_t \widehat{F}^T(\hat{\theta}_L^{(t-1)}) (\hat{\theta}_L^{(t-1)} - \theta_L^*) + \frac{1}{2} \gamma_t^2 \|\widehat{F}^T(\hat{\theta}_L^{(t-1)})\|_2^2.
\end{aligned}$$

Taking expectation of both sides with respect to \mathcal{D}^{Tr} yields

$$\begin{aligned}
d_t &\leq \frac{1}{2} d_{t-1} - \gamma_t \mathbb{E}_{\mathcal{D}^{\text{Tr}}} \left[\widehat{F}^T(\hat{\theta}_L^{(t-1)}) (\hat{\theta}_L^{(t-1)} - \theta_L^*) \right] + 2\gamma_t^2 M^2 \\
&\leq (1 - 2\kappa\gamma_t) d_{t-1} + 2\gamma_t^2 M^2,
\end{aligned}$$

where the last inequality follows by noting that \widehat{F} is an unbiased estimator of F , which satisfies

$$F(\theta_L)^T (\theta_L - \theta_L^*) \geq \kappa \|\theta_L - \theta_L^*\|_2,$$

due to $F(\theta_L^*) = 0$. Then, using triangle inequality yields the result.

Lastly, we prove by induction that if we define $R = (2M^2)/\kappa^2$, $\gamma_t = 1/\kappa(t+1)$, we have

$$d_t \leq \frac{R}{t+1}.$$

(Base case when $t = 0$.) Let B be the $\|\cdot\|_2$ diameter of Θ (e.g., $\|\theta_1 - \theta_2\|_2^2 \leq B^2 \forall (\theta_1, \theta_2) \in \Theta$). Denote $\theta_L^+, \theta_L^- \in \mathcal{B}$ to satisfy $\|\theta_L^+ - \theta_L^-\|_2^2 = B^2$. By the definition of κ ,

$$\langle F(\theta_L^+) - F(\theta_L^-), \theta_L^+ - \theta_L^- \rangle \geq \kappa \|\theta_L^+ - \theta_L^-\|_2^2 = \kappa B^2.$$

Meanwhile, the Cauchy-Schwarz inequality yields

$$\langle F(\theta_L^+) - F(\theta_L^-), \theta_L^+ - \theta_L^- \rangle = \langle \eta^*(X)(\phi_L(\eta^*(X))\theta_L^+) - \eta^*(X)(\phi_L(\eta^*(X))\theta_L^-), \theta_L^+ - \theta_L^- \rangle \leq 2MB.$$

Thus, $B \leq 2M/\kappa$. As a result, $B^2/2 \leq 2M^2/\kappa^2 = R$. Because $d_0 = \|\hat{\theta}_L^{(0)} - \theta_L^*\|_2^2 \leq B^2$,

$$d_0 \leq 2R = \frac{4M^2}{\kappa^2}.$$

(The inductive step from $t-1$ to t .) Note that by the definition of γ_t , $\kappa\gamma_t = 1/(t+1) \leq 1/2$. Thus,

$$\begin{aligned}
d_t &\leq (1 - 2\kappa\gamma_t) d_{t-1} + 2\gamma_t^2 M^2 \\
&= \frac{R}{t} \left(1 - \frac{2}{t+1}\right) + \frac{R}{(t+1)^2} \leq \frac{R}{t+1},
\end{aligned}$$

whereby the proof is complete by the definition of d_t and R . □

Proof of Theorem 4.3. We have that

$$\begin{aligned}
& \mathbb{E}_{X, \mathcal{D}^{\text{Tr}}} \{ \|\widehat{Y}(X, \widehat{\theta}_L^{(T)}) - \mathbb{E}[Y|X]\|_2^2 \} \\
&= \mathbb{E}_{X, \mathcal{D}^{\text{Tr}}} \{ \|\phi_L(X_L^* \widehat{\theta}_L^{(T)}) - \phi_L(X_L^* \theta_L^*)\|_2^2 \} \\
&\stackrel{(i)}{\leq} \mathbb{E}_{X, \mathcal{D}^{\text{Tr}}} \{ K^2 \|X_L^* \widehat{\theta}_L^{(T)} - X_L^* \theta_L^*\|_2^2 \} \\
&= \mathbb{E}_{X, \mathcal{D}^{\text{Tr}}} \{ K^2 [\widehat{\theta}_L^{(T)} - \theta_L^*]^T X_L^{*\top} X_L^* [\widehat{\theta}_L^{(T)} - \theta_L^*] \} \\
&\stackrel{(ii)}{=} \mathbb{E}_{\mathcal{D}^{\text{Tr}}} \{ K^2 [\widehat{\theta}_L^{(T)} - \theta_L^*]^T \mathbb{E}_X \{ X_L^{*\top} X_L^* \} [\widehat{\theta}_L^{(T)} - \theta_L^*] \} \\
&\leq K^2 \lambda_{\max}(E_X \{ X_L^{*\top} X_L^* \}) \mathbb{E}_{\mathcal{D}^{\text{Tr}}} \{ \|\widehat{\theta}_L^{(T)} - \theta_L^*\|_2^2 \},
\end{aligned}$$

where (i) holds by K -Lipschitz assumption on ϕ_L and (ii) holds by the independence of X (as a new feature) and $\widehat{\theta}_L^{(T)}$ (depending on training data only). We can then use the bound on $\mathbb{E}_{\mathcal{D}^{\text{Tr}}} \{ \|\widehat{\theta}_L^{(T)} - \theta_L^*\|_2 \}$ from the previous lemma to complete the proof. \square

Proof of Theorem 4.5. For a given $\theta_L \in \Theta$, let $N_{\Theta}(\theta_L) = \{y \in \mathbb{R}^p | \langle y, \theta' - \theta_L \rangle, \forall \theta' \in \Theta\}$ denote the normal cone of Θ at θ_L . The first step is to bound the expected value of the norm of F evaluated at the stochastic OE estimate. This bound results from [Kotsalis et al., 2022, Theorem 3.8], where for any $\theta_L \in \Theta$, the residual

$$\mathbb{E}[\text{res}(\theta_L)] \leq \epsilon, \quad \text{res}(\theta_L) = \min_{y \in -N_{\Theta}(\theta_L)} \|y - F(\theta_L)\|_2$$

acts as the termination criteria for the recurrence under a certain choice of the Bregman's distance $V(a, b)$; we let $V(a, b) = \|a - b\|_2^2/2$ in our case.

Under assumptions on F and choices of step sizes, we can thus restate [Kotsalis et al., 2022, Theorem 3.8] in our special case as

$$\mathbb{E}_{\mathcal{D}^{\text{Tr}}} [\text{res}(\widehat{\theta}_L^{(R)})] \leq \frac{3\sigma}{\sqrt{T}} + \frac{12K_2 \sqrt{2\|\theta_L^*\|_2^2 + \frac{2\sigma^2}{L^2}}}{\sqrt{T}}.$$

When Θ is the entire space, $N_{\Theta}(\theta_L) = \{0\}$. As a result, $\text{res}(\widehat{\theta}_L^{(R)}) = \|F(\widehat{\theta}_L^{(R)})\|_2$.

Furthermore, recall the fact that for a matrix $A \in \mathbb{R}^{m \times n}$ and vectors $x, x' \in \mathbb{R}^n$, we have

$$\|x - x'\|_2 \leq \|A(x - x')\|_2 / \sigma_{\min}(A),$$

where $\sigma_{\min}(A)$ denotes the smallest singular value of A . Thus, by letting $A = \eta^*(X)$, $x = \widehat{Y}(X, \widehat{\theta}_L^{(R)})$, $x' = \mathbb{E}[Y|X]$ we have in expectation that

$$\mathbb{E}_{\mathcal{D}^{\text{Tr}}} \{ \|\mathbb{E}_X \{ \sigma_{\min}(\eta^*(X)) [\widehat{Y}(X, \widehat{\theta}_L^{(R)}) - \mathbb{E}[Y|X]] \}\|_2 \} \leq \mathbb{E}_{\mathcal{D}^{\text{Tr}}} \|F(\widehat{\theta}_L^{(R)})\|_2,$$

where we used the fact $F(\widehat{\theta}_L^{(R)}) = \mathbb{E}_{X, Y} \{ \eta^*(X)^{\top} [\phi_L(\eta^*(X) \widehat{\theta}_L^{(R)}) - Y] \} = \mathbb{E}_X \{ \eta^*(X)^{\top} [\widehat{Y}(X, \widehat{\theta}_L^{(R)}) - \mathbb{E}[Y|X]] \}$. \square

Proof of Proposition 4.6. For notation simplicity, denote $\eta = \eta^*(X)$ and $\theta = \theta_L$. Meanwhile, for two vectors $a, b \in \mathbb{R}^n$, the notation a/b denotes the point-wise division. $\mathbf{1}$ denotes a vector of all 1.

We first consider the binary cross-entropy loss $\mathcal{L}(Y, \theta_L)$ defined in (9). Note that we have

$$\begin{aligned}\mathcal{L}(Y, \theta_L) &= -Y \log(\phi_L(\eta^*(X)\theta_L)) - (1 - Y) \log(1 - \phi_L(\eta^*(X)\theta_L)) \\ &= -Y^T \log(\exp(\eta\theta)/(\mathbf{1} + \exp(\eta\theta))) - (\mathbf{1} - Y)^T \log(\mathbf{1}/(\mathbf{1} + \exp(\eta\theta))) \\ &= -Y^T \eta\theta + Y^T \log(\mathbf{1} + \exp(\eta\theta)) + (\mathbf{1} - Y)^T \log(\mathbf{1} + \exp(\eta\theta)) \\ &= \mathbf{1}^T \log(\mathbf{1} + \exp(\eta\theta)) - Y^T \eta\theta.\end{aligned}$$

Thus, the gradient with respect to θ can be written as

$$\nabla_{\theta} \mathcal{L}(Y, \theta_L) = \eta^T \frac{\exp(\eta\theta)}{\mathbf{1} + \exp(\eta\theta)} - \eta^T Y = \eta^*(X)^T [\phi_L(\eta^*(X)\theta_L) - Y].$$

Taking expectation thus yields the result.

We next consider the categorical cross-entropy loss $\mathcal{L}(Y, \theta_L)$ defined in (10). Note that we have

$$\begin{aligned}\mathcal{L}(Y, \theta_L) &= -e_Y^T \log(\phi_L(\eta^*(X)\theta_L)) \\ &= \left[-e_Y^T \log \left(\frac{\exp(\eta\theta)}{\mathbf{1}^T \exp(\eta\theta)} \right) \right] \\ &= -e_Y^T (\eta\theta) + \log(\mathbf{1}^T \exp(\eta\theta)).\end{aligned}$$

Thus, the gradient with respect to θ can be written as

$$\begin{aligned}\nabla_{\theta} \mathcal{L}(Y, \theta) &= -\eta^T e_Y + \eta^T \frac{\exp(\eta\theta)}{\mathbf{1}^T \exp(\eta\theta)} \\ &= \eta^T [\phi_L(\eta\theta) - e_Y] = \eta^*(X)^T [\phi_L(\eta^*(X)\theta_L) - Y],\end{aligned}$$

where in the definition of $F(\theta)$ in (3), $Y = e_Y \in \mathbb{R}^{k+1}$ if Y belongs to more than 2 classes. Taking expectation thus yields the result. \square